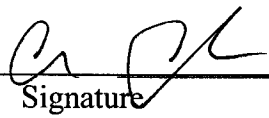


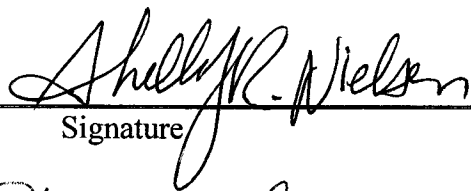
560069

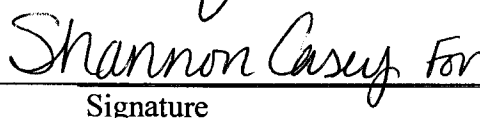
**Sandia National Laboratories
Waste Isolation Pilot Plant**

**Analysis Package for Direct Brine Releases:
CRA-2014 Performance Assessment (CRA-2014 PA)**

Author: Bwalya Malama  05/15/2013
Print Signature Date

Technical
Review: Chris Camphouse  5/15/2013
Print Signature Date

QA
Review: Shelly R. Nielsen  5-15-13
Print Signature Date

Management
Review: Sean Dunagan  5/15/13
Print Signature Date

WIPP:1.2.5:PA:QA-L:559199

Information Only

Table of Contents

1 Introduction.....6

2 Background.....7

3 Approach.....9

 3.1 Model Geometry.....9

 3.2 Initial Conditions.....11

4 Calculation Methodology.....12

 4.1 Modeled Scenarios.....13

 4.1.1 Scenario 1 (S1-DBR).....13

 4.1.2 Scenario 2 (S2-DBR).....13

 4.1.3 Scenario 3 (S3-DBR).....14

 4.1.4 Scenario 4 (S4-DBR).....14

 4.1.5 Scenario 5 (S5-DBR).....15

 4.2 Run Control.....15

5 Results.....15

 5.1 Summary.....16

 5.2 Direct Brine Releases from the Lower Drilling Location.....18

 5.3 Sensitivity of Direct Brine Releases to Input Parameters.....40

6 Conclusions.....46

7 References.....47

Information Only

List of Tables

Table 2-1: Summary of parameters used to compute DBR volumes.....	8
Table 4-1: Scenarios used in BRAGFLO Salado flow modeling.....	13
Table 4-2: Intrusion times modeled by DBR for each scenario.....	13
Table 5-1: Summary statistics for case CRA-14BL of the CRA-2014 PA and PABC-2009 DBR calculations for replicate 1 over all vectors.	17
Table 5-2: Summary statistics for the CRA-2014 PA and PABC-2009 DBR calculations for all replicates and all vectors.....	17
Table 5-3: Case CRA14-BL and PABC-2009 summary statistics of the DBR volumes for replicate 1 for the S1-DBR calculations.	19
Table 5-4: Case CRA14-0 and PABC-2009 summary statistics of the DBR volumes for all replicates for the S1-DBR calculations.....	20
Table 5-5: Case CRA14-BL and PABC-2009 summary statistics of the DBR volumes for replicate 1 for the S2-DBR calculations.	21
Table 5-6: Case CRA14-0 and PABC-2009 summary statistics of the DBR volumes for all replicates for the S2-DBR calculations.....	22
Table 5-7: Case CRA14-BL and PABC-2009 summary statistics of the DBR volumes for replicate 1 for the S3-DBR calculations.	23
Table 5-8: Case CRA14-0 and PABC-2009 summary statistics of the DBR volumes for all replicates for the S3-DBR calculations.....	24
Table 5-9: Case CRA14-BL and PABC-2009 summary statistics of the DBR volumes for replicate 1 for the S4-DBR calculations.	25
Table 5-10: Case CRA14-0 and PABC-2009 summary statistics of the DBR volumes for all replicates for the S4-DBR calculations.....	26
Table 5-11: Case CRA14-BL and PABC-2009 summary statistics of the DBR volumes for replicate 1 for the S5-DBR calculations.	27
Table 5-12: Case CRA14-0 and PABC-2009 summary statistics of the DBR volumes for all replicates for the S5-DBR calculations.....	28

List of Figures

Figure 3-1: CRA-2014 PA DBR material map (logical grid) with ROMPCS.	10
Figure 3-2: PABC-2009 DBR material map (logical grid) with Option D panel closure (after Clayton et al., 2010).....	11
Figure 5-1: Plot of the percentile (x-axis) of DBR volumes that are less than the DBR volume on the y-axis for case CRA14-BL of the CRA-2014 PA at the lower intrusion location for replicate 1; scenario S1-DBR.....	30
Figure 5-2: Plot of the percentile (x-axis) of DBR volumes that are less than the DBR volume on the y-axis for the PABC-2009 at the lower intrusion location for replicate 1; scenario S1-DBR.	30
Figure 5-3: Plot of the percentile (x-axis) of DBR volumes that are less than the DBR volume on the y-axis for case CRA14-0 of the CRA-2014 PA at the lower intrusion location over all replicates; scenario S1-DBR.	31

Figure 5-4: Plot of the percentile (x-axis) of DBR volumes that are less than the DBR volume on the y-axis for the PABC-2009 at the lower intrusion location for all replicates; scenario S1-DBR. 31

Figure 5-5: Plot of the percentile (x-axis) of DBR volumes that are less than the DBR volume on the y-axis for case CRA14-BL of the CRA-2014 PA at the lower intrusion location for replicate 1; scenario S2-DBR..... 32

Figure 5-6: Plot of the percentile (x-axis) of DBR volumes that are less than the DBR volume on the y-axis for the PABC-2009 at the lower intrusion location for replicate 1; scenario S2-DBR. 32

Figure 5-7: Plot of the percentile (x-axis) of DBR volumes that are less than the DBR volume on the y-axis for case CRA14-0 of the CRA-2014 PA at the lower intrusion location for all replicates; scenario S2-DBR. 33

Figure 5-8: Plot of the percentile (x-axis) of DBR volumes that are less than the DBR volume on the y-axis for the PABC-2009 at the lower intrusion location for replicate 1; scenario S2-DBR. 33

Figure 5-9: Plot of the percentile (x-axis) of DBR volumes that are less than the DBR volume on the y-axis for case CRA14-BL of the CRA-2014 PA at the lower intrusion location for replicate 1; scenario S3-DBR..... 34

Figure 5-10: Plot of the percentile (x-axis) of DBR volumes that are less than the DBR volume on the y-axis for the PABC-2009 at the lower intrusion location for replicate 1; scenario S3-DBR. 34

Figure 5-11: Plot of the percentile (x-axis) of DBR volumes that are less than the DBR volume on the y-axis for case CRA14-0 of the CRA-2014 PA at the lower intrusion location for all replicates; scenario S3-DBR. 35

Figure 5-12: Plot of the percentile (x-axis) of DBR volumes that are less than the DBR volume on the y-axis for the PABC-2009 at the lower intrusion location for all replicates; scenario S3-DBR..... 35

Figure 5-13: Plot of the percentile (x-axis) of DBR volumes that are less than the DBR volume on the y-axis for case CRA14-BL of the CRA-2014 PA at the lower intrusion location for replicate 1; scenario S4-DBR..... 36

Figure 5-14: Plot of the percentile (x-axis) of DBR volumes that are less than the DBR volume on the y-axis for the PABC-2009 at the lower intrusion location for replicate 1; scenario S4-DBR. 36

Figure 5-15: Plot of the percentile (x-axis) of DBR volumes that are less than the DBR volume on the y-axis for case CRA14-0 of the CRA-2014 PA at the lower intrusion location for all replicates; scenario S4-DBR..... 37

Figure 5-16: Plot of the percentile (x-axis) of DBR volumes that are less than the DBR volume on the y-axis for the PABC-2009 at the lower intrusion location for all replicates; scenario S4-DBR..... 37

Figure 5-17: Plot of the percentile (x-axis) of DBR volumes that are less than the DBR volume on the y-axis for case CRA14-BL of the CRA-2014 PA at the lower intrusion location for replicate 1; scenario S5-DBR..... 38

Figure 5-18: Plot of the percentile (x-axis) of DBR volumes that are less than the DBR volume on the y-axis for the PABC-2009 at the lower intrusion location for replicate 1; scenario S5-DBR. 38

Figure 5-19: Plot of the percentile (x-axis) of DBR volumes that are less than the DBR volume on the y-axis for case CRA14-0 of the CRA-2014 PA at the lower intrusion location for all replicates; scenario S5-DBR. 39

Figure 5-20: Plot of the percentile (x-axis) of DBR volumes that are less than the DBR volume on the y-axis for the PABC-2009 at the lower intrusion location for all replicates; scenario S5-DBR. 39

Figure 5-21: Scatter plot of DBR volume versus pressure in intruded panel for S2-DBR scenario, lower drilling intrusion, case CRA14-BL. Symbols indicate intrusion times in years. 41

Figure 5-22: Scatter plot of DBR volume versus pressure in intruded panel for S2-DBR scenario, lower drilling intrusion, case CRA14-0. Symbols indicate intrusion times in years. 42

Figure 5-23: Scatter plot of DBR volume versus pressure in intruded panel for S2-DBR scenario, lower drilling intrusion, PABC-2009. Symbols indicate intrusion times in years. 42

Figure 5-24: Scatter plot of DBR volume versus pressure in the intruded panel for replicate 1, S2-DBR scenario, lower drilling intrusion, CRA14-BL PA. Symbols indicate the range of mobile brine saturation (dimensionless). 43

Figure 5-25: Scatter plot of DBR volume versus pressure in the intruded panel for replicate 1, S2-DBR scenario, lower drilling intrusion, CRA-2014 PA. Symbols indicate the range of mobile brine saturation (dimensionless). 43

Figure 5-26: Scatter plot of DBR volume versus pressure in the intruded panel for replicate 1, S2-DBR scenario, lower drilling intrusion, PABC-2009. Symbols indicate the range of mobile brine saturation (dimensionless). 44

Figure 5-27: Scatter plot of mobile brine saturation versus pressure for replicate 1, S2-DBR scenario, lower drilling intrusion, all intrusion times, CRA14-BL PA. Symbols indicate the range of DBR volumes in m³. 44

Figure 5-28: Scatter plot of mobile brine saturation versus pressure for replicate 1, S2-DBR scenario, lower drilling intrusion, all intrusion times, CRA-2014 PA. Symbols indicate the range of DBR volumes in m³. 45

Figure 5-29: Scatter plot of mobile brine saturation versus pressure for replicate 1, S2-DBR scenario, lower drilling intrusion, all intrusion times, PABC-2009. Symbols indicate the range of DBR volumes in m³. 45

1 INTRODUCTION

The Waste Isolation Pilot Plant (WIPP), located in southeastern New Mexico, has been developed by the U.S. Department of Energy (DOE) for the geologic (deep underground) disposal of transuranic (TRU) waste. Containment of TRU waste at the WIPP is regulated by the U.S. Environmental Protection Agency (EPA) according to the regulations set forth in Title 40 of the Code of Federal Regulations (CFR), Part 191. The DOE demonstrates compliance with the containment requirements according to the Certification Criteria in Title 40 CFR Part 194 by means of performance assessment (PA) calculations performed by Sandia National Laboratories (SNL). WIPP PA calculations estimate the probability and consequence of potential radionuclide releases from the repository to the accessible environment for a regulatory period of 10,000 years after facility closure. The models used in PA are maintained and updated with new information as part of an ongoing process. Improved information regarding important WIPP features, events, and processes typically results in refinements and modifications to PA models and the parameters used in them. Planned changes to the repository and/or the components therein also result in updates to WIPP PA models. WIPP PA models are used to support the repository recertification process that occurs at five-year intervals following the receipt of the first waste shipment at the site in 1999.

PA calculations were included in the 1996 Compliance Certification Application (CCA) (U.S. DOE 1996), and in a subsequent Performance Assessment Verification Test (PAVT) (MacKinnon and Freeze 1997a, 1997b and 1997c). Based in part on the CCA and PAVT PA calculations, the EPA certified that the WIPP met the regulatory containment criteria. The facility was approved for disposal of transuranic waste in May 1998 (U.S. EPA 1998). PA calculations were an integral part of the 2004 Compliance Recertification Application (CRA-2004) (U.S. DOE 2004). During their review of the CRA-2004, the EPA requested an additional PA calculation, referred to as the CRA-2004 Performance Assessment Baseline Calculation (PABC) (Leigh et al. 2005), be conducted with modified assumptions and parameter values (Cotsworth 2005). Following review of the CRA-2004 and the CRA-2004 PABC, the EPA recertified the WIPP in March 2006 (U.S. EPA 2006).

PA calculations were completed for the second WIPP recertification and documented in the 2009 Compliance Recertification Application (CRA-2009). The CRA-2009 PA resulted from continued review of the CRA-2004 PABC, including a number of technical changes and corrections, as well as updates to parameters and improvements to the PA computer codes (Clayton et al., 2008). To incorporate additional information which was received after the CRA-2009 PA was completed, but before the submittal of the CRA-2009, the EPA requested an additional PA calculation, referred to as the 2009 Compliance Recertification Application Performance Assessment Baseline Calculation (PABC-2009) (Clayton et al., 2010), be undertaken which included updated information (Cotsworth, 2009). Following the completion and submission of the PABC-2009, the WIPP was recertified in 2010 (U.S. EPA 2010).

The Land Withdrawal Act (U.S. Congress 1992) requires that the DOE apply for WIPP recertification every five years following the initial 1999 waste shipment. The 2014 Compliance Recertification Application (CRA-2014) is the third WIPP recertification application submitted by the DOE for EPA approval. The PA executed by SNL in support of the CRA-2014 is detailed

in AP-164 (Camphouse 2013a). The CRA-2014 PA includes a number of technical changes and parameter refinements, as well as a redesigned WIPP panel closure system. Results found in the CRA-2014 PA are compared to those obtained in the PABC-2009 in order to assess repository performance in terms of the current regulatory baseline. This analysis package documents the direct brine releases (DBRs) component of the CRA-2014 PA analysis.

2 BACKGROUND

DBRs refer to flow of contaminated brine, from the repository, to land surface through an intrusion borehole during the period of drilling. In order for a DBR to occur, two criteria must be satisfied (Stoelzel and O'Brien 1996), namely

1. Brine pressure in the repository in the vicinity of the intrusion must exceed the drilling fluid hydrostatic pressure (estimated to be 8 MPa).
2. Brine saturation in the repository must exceed the residual brine saturation of the waste material. The residual brine saturation is sampled from a uniform distribution ranging from 0.0 to 0.552.

If both of these criteria are satisfied, a DBR is calculated, otherwise no DBR is calculated. DBR computations are performed by the numerical multi-phase fluid flow code, BRAGFLO, using a two dimensional, near-horizontal grid. The grid dips 1° to the south, and represents the vicinity of the waste panels. The BRAGFLO code computes DBR volumes using the well deliverability equation given by (Mattax and Dalton 1990)

$$q_p(t) = J_p [P_p(t) - P_{wf}] \quad (1)$$

where $q_p(t)$ is the volumetric brine flux to the well as a function of time, t , J_p is the well productivity index, $P_p(t)$ is the volume averaged brine pressure of the repository in the vicinity of the intrusion as a function of time, and P_{wf} is the flowing bottom-hole pressure (assumed to be constant during each drilling intrusion). The flowing bottom-hole pressure is defined as the dynamic pressure at the inlet to the wellbore adjacent to the point of entry into the repository. It is less than the static panel pressure (P_p) due to elevation, friction and acceleration effects (Stoelzel and O'Brien 1996).

The well productivity index, J_p , is a measure of how readily brine can flow through the panel and enter the well then flow to land surface. It is calculated according to (Mattax and Dalton 1990; Chappellear and Williamson 1981)

$$J_p = \frac{2\pi k k_{rp} h}{\mu [\ln(r_e/r_w) + s + 0.5]} \quad (2)$$

where k is intrinsic permeability of the waste, k_{rp} is relative brine permeability of the waste, h is the crushed panel height, μ is brine dynamic viscosity, r_e is the equivalent drainage radius of the grid block containing the well, r_w is well radius, and s is the skin factor.

To compute the results reported herein, the waste area intrinsic permeability is fixed at $k = 2.4 \times 10^{-13} \text{ m}^2$. Relative permeability is computed using the model of Brooks and Corey (1964) given by

$$k_{rp} = S_e^{3+2/\lambda} \quad (3)$$

where λ is the pore distribution parameter, $S_e = (S_b - S_{br})/(1 - S_{br})$ is the effective brine saturation, S_b is the brine saturation, and S_{br} is the residual brine saturation.

The crushed panel height is defined as $h = h_i(1 - \phi_i)/(1 - \phi)$, where h_i is initial panel height (fixed at 3.96 m), ϕ_i is the initial room-scale porosity, and ϕ is the room-scale porosity at the time of intrusion, which is calculated by BRAGFLO (see Helton et al. 1998). The effective drainage radius is defined by $r_e = \sqrt{\Delta x \Delta y / \pi}$, where Δx and Δy are the dimensions of the grid cell containing the well. The wellbore radius is fixed at 0.1556 m, which is based on the assumption of a 12.25 in. drill bit diameter.

Assuming an infinite (open channel) permeability for the intruding borehole, the skin factor, which accounts for enhanced well productivity due to the presence of a cavity at the base of the well, is given by $s = \ln(r_w/r_s)$ (Lee 1982) where r_s is the effective radius of the well bore with the cuttings, cavings and spillings of total volume V_i removed. Hence, equation (2) reduces to

$$J_p = \frac{2\pi h k k_{rp}}{\mu_p [\ln(r_e/r_s) - 1/2]} \quad (4)$$

The effective radius r_s is obtained by converting the volume V_i into an equivalent cylinder of volume V_i and height h_i , and then computing the radius of the cylinder as $r_s = \sqrt{V_i/(\pi h_i)}$.

The parameter values used to compute the DBR volumes are summarized in Table 2-1. Five scenarios were simulated and are discussed in section 4.1.

Table 2-1. Summary of parameters used to compute DBR volumes

Parameter	Name in BRAGFLO	Description	Value
k	PRMX	Intrinsic Permeability	$2.4 \times 10^{-13} \text{ m}^2$ (fixed)
λ	PORE_DIS	Brooks-Corey parameter	2.89
S_{br}	SAT_RBRN	Residual brine saturation	Varies
ϕ_i	POROSITY	Initial panel porosity	0.848
μ	VISCO	Brine dynamic viscosity	0.0021 Pa-s

3 APPROACH

The conceptual models implemented in the CRA-2014 PA calculations are unchanged from those used in the PABC-2009 (Clayton et al., 2010). The set of changes since PABC-2009 that are incorporated in the CRA-2014 PA are detailed in Camphouse (2013a), and are summarized as follows:

1. Replacement of the “Option D” panel closure system with a Run-of-Mine panel closure system (ROMPCS);
2. Inclusion of an additional mined region in the north end of the repository;
3. Update of waste inventory parameters;
4. Update of radionuclide solubilities and their associated uncertainty;
5. Update of drilling rate and plugging pattern parameters;
6. Refinement of parameters BOREHOLE:TAUFAIL and GLOBAL:PBRINE;
7. Variable brine volume implementation;
8. Update of iron corrosion rate parameter, and;
9. Implementation of a refined water balance to include MgO hydration.

Of the changes listed above, the implementation of the ROMPCS, increase in the mined-out region, and update of waste inventory parameters. Additionally, because of its effect on gas generation and waste panel brine saturation, the changes to the iron corrosion rate and the refined water balance implementation can also impact DBR volumes.

The results of the CRA-2014 PA DBR computations will be compared to those of the PABC-2009 to assess the impact of these and the other parameter and implementation changes discussed in detail in Camphouse (2013a). The CRA-2014 PA model runs discussed herein are for the two cases referred to as CRA14-BL and CRA14-0 in in Camphouse (2013a). Case CRA14-BL is used to assess the impact of changes 1 through 5 listed above and referred to as baseline changes. For this case only one replicate was executed. Case CRA14-0 assesses the impact of all changes listed above for inclusion in the CRA-2014 PA. Thus, in addition to the baseline changes, case CRA14-0 includes effects of changes 6 through 9, namely update of parameters BOREHOLE:TAUFAIL and GLOBAL:PBRINE, implementation of variable brine volume, update of iron corrosion rate, and refinement of the repository water balance (Camphouse 2013a). All three replicates were executed for case CRA14-0.

3.1 Model Geometry

The scenarios used for the CRA-2014 PA are the same as those used for the PABC-2009. The DBR numerical grid and material map used in the CRA-2014 PA calculations is shown in Figure 3-1. Note that the color scheme in Figure 3-1 has been chosen so as to correspond to the color scheme used in the PCS-2012 PA BRAGFLO grid and material map (Camphouse 2012b). The PABC-2009 DBR numerical grid and material map is shown in Figure 3-2 for comparison.

The Option D panel closure modeled in the PABC-2009 is 40 meters long whereas the Run-of-Mine Panel Closure System (ROMPCS) used in the CRA-2014 PA is 30.48 meters (100 feet) long. As a result, grid cell lengths corresponding to panel closures were reduced to 30.48 meters

in the CRA-2014 PA. In addition, the ROMPCS has no concrete component that is “keyed in” to the surrounding Disturbed Rock Zone (DRZ). As a result, material elements corresponding to equivalent DRZ/concrete in the PABC-2009 are replaced by DRZ in the CRA-2014 PA.

To calculate DBR volumes the same three drilling locations considered in PABC-2009 are considered in the CRA-2014 PA, namely: upper (up-dip), middle, and lower (down-dip) locations. They are shown in Figure 3-1 (compare with Figure 3-2 for the PABC-2009). Some of the DBR calculations are for a drilling intrusion preceded by an earlier intrusion in either the same or a different waste panel. The effects of these prior intrusions are incorporated into the calculations by specifying a boundary or initial condition well at their grid location, denoted by the red dot in Figure 3-1. The properties of the boundary condition will depend on the type of the prior intrusion and the amount of time that has elapsed since its occurrence.

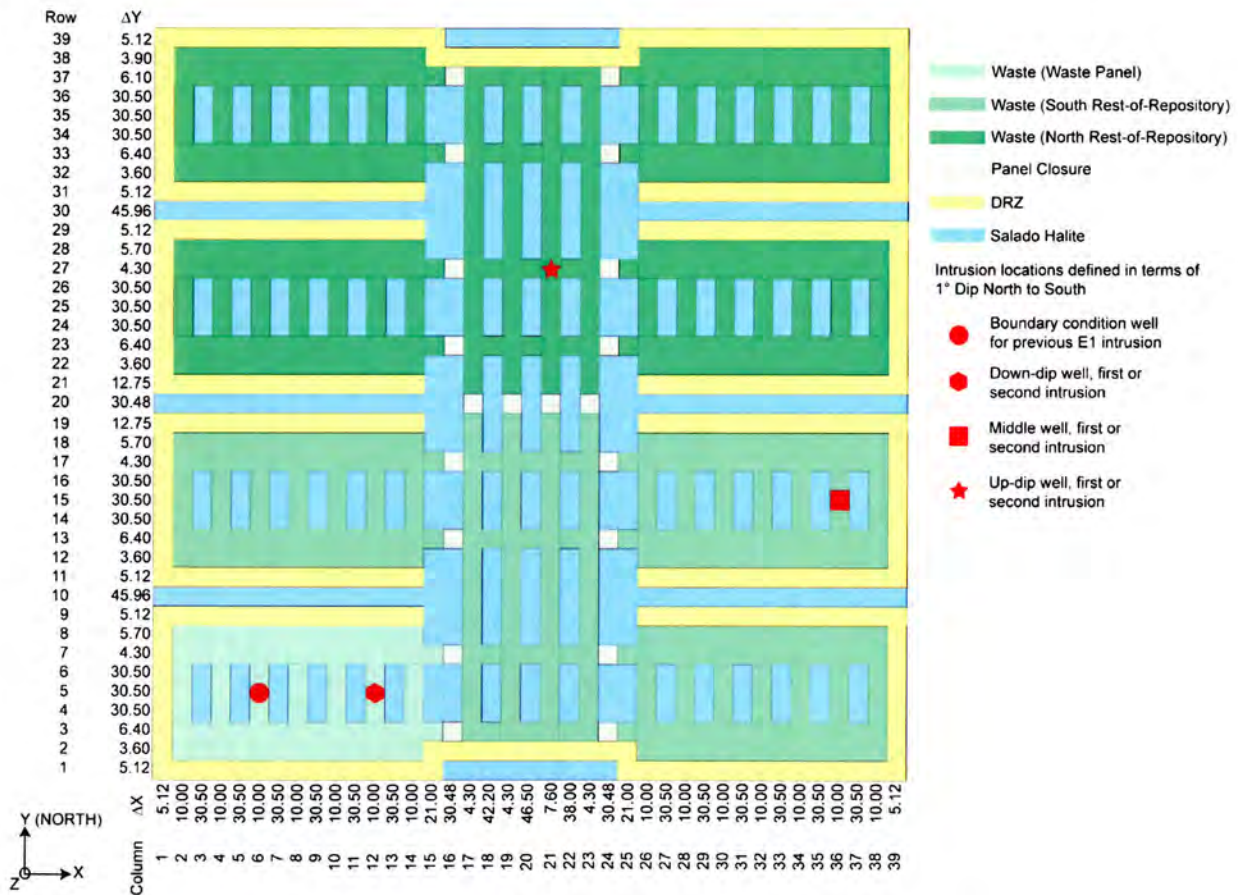


Figure 3-1: CRA-2014 PA DBR material map (logical grid) with ROMPCS.

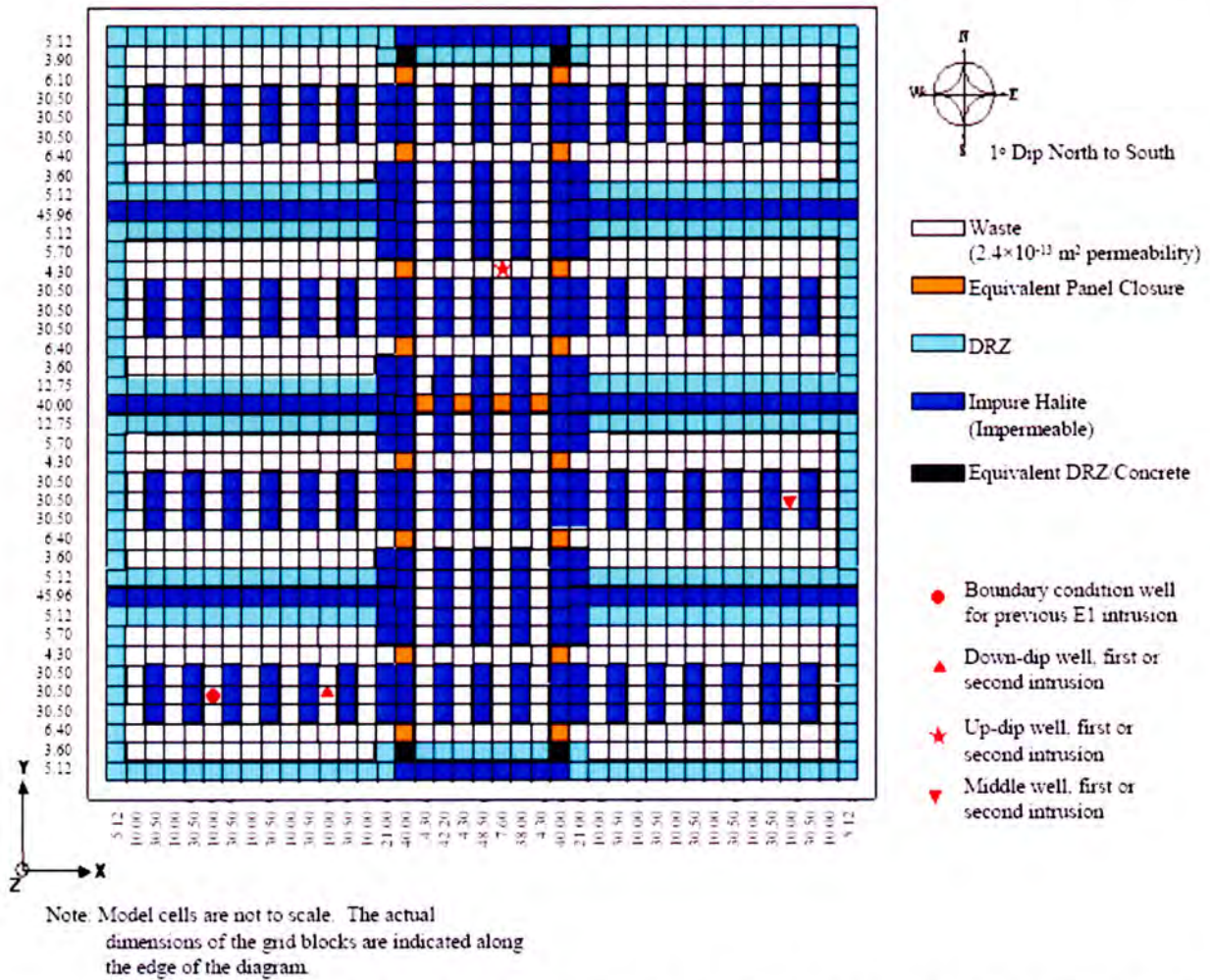


Figure 3-2: PABC-2009 DBR material map (logical grid) with Option D panel closure (after Clayton et al., 2010).

3.2 Initial Conditions

Volume averaged brine pressures and brine saturations are calculated from the 10,000 year BRAGFLO simulations. The BRAGFLO results, corresponding to the time of intrusion, are used in the DBR simulations as initial conditions. The waste regions in the BRAGFLO grid and the DBR grid are each divided into three regions and volume-averaged brine pressure and saturations are transferred from corresponding regions in the BRAGFLO grid to the DBR grid. These regions corresponded to the single waste panel, south rest of repository (SRR), and north rest of repository (NRR). This method of mapping the waste regions from the BRAGFLO grid to the BRAGFLO-DBR grid ensures that the relative volumes of these regions are equal between the 10,000 year BRAGFLO runs and the DBR runs. The definitions of these repository regions are included in Figure 3-1.

Figure 3-4 illustrates the method used to transfer initial conditions in the waste for the CRA-2014 PA, which is unchanged from the PABC-2009 DBR runs. The volume averaged pressure and saturation from the three waste-filled regions in the BRAGFLO grid (WAS_AREA, SRR, NRR) at the time of the intrusion are used as the initial pressure and saturation for the three waste regions in the DBR grid (Lower, Middle, and Upper, respectively). The pressure and saturation are allowed to change during the DBR calculations.

4 CALCULATION METHODOLOGY

DBR calculations are divided into five scenarios. Each DBR scenario represents an intrusion into the repository due to a drilling event. The initial conditions for the DBR simulations are obtained from the BRAGFLO Salado Flow simulations (Camphouse, 2013b) using an appropriate scenario and at an appropriate time for the particular drilling intrusion time. An E1 intrusion scenario is defined as an intrusion into the repository, which creates a pathway to a pressurized brine pocket below the repository. An E2 intrusion scenario is defined as one that terminates in the repository without creating a pathway to an underlying pressurized brine pocket. The results of DBR calculations are the volumes of brine emanating from the repository and reaching the surface at the time of drilling and up to 4.5 days after. These results are used by the code CCDFGF to interpolate volumes of waste for the specific conditions that arise in a given future (location and timing of future drilling intrusions).

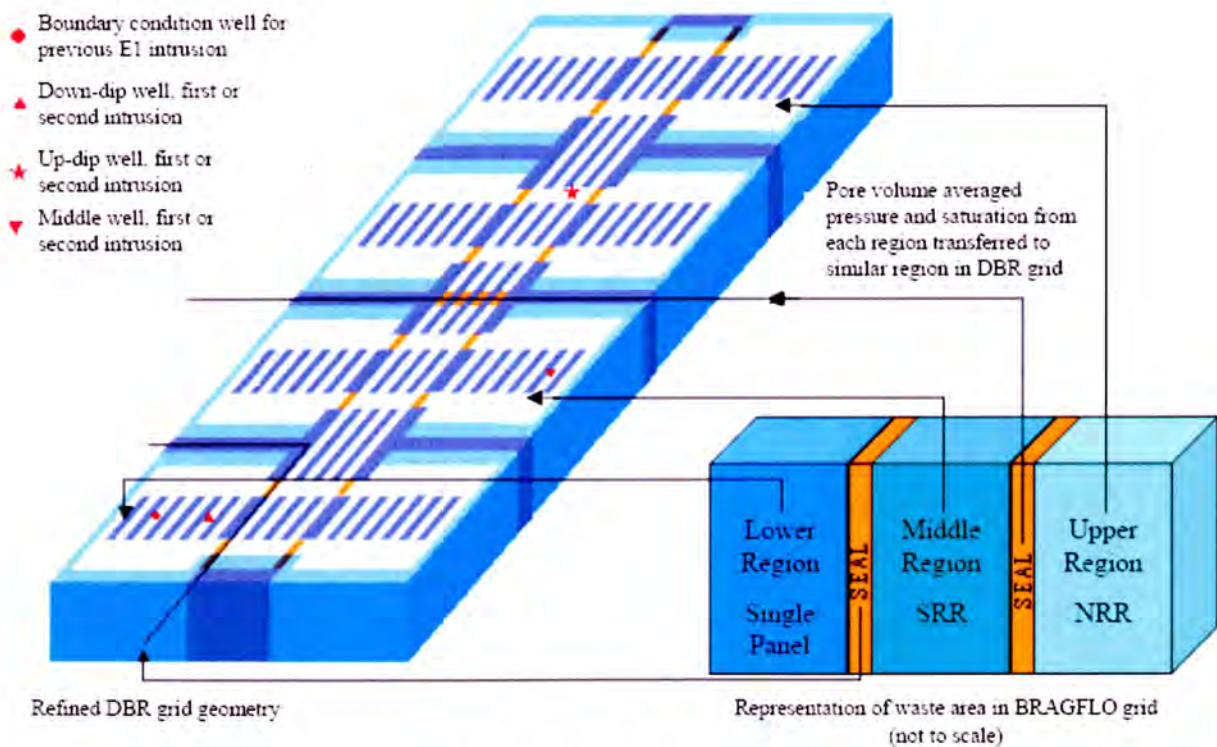


Figure 3-4. Regions to be used to transfer initial pressure and saturation from the 10,000 year BRAGFLO grid to the DBR grid for the CRA-2014.

4.1 Modeled Scenarios

In the following, an overview of the DBR calculations performed for the CRA-2014 PA is given. In performing DBR calculations, the five BRAGFLO scenarios S1-BF to S5-BF used in Salado flow modeling are used to set brine pressure and saturation in the DBR calculations at the time of intrusion. The BRAGFLO Salado flow scenarios are summarized in Table 4-1.

With brine pressure and saturation transferred from the Salado flow results, DBR calculations quantify impacts due to an initial or subsequent intrusion into the repository. DBR simulations cover a range of intrusion scenarios, locations, and timing using five scenarios, S1-DBR to S5-DBR. A summary of intrusion times for each DBR scenario is given in Table 4-2.

Table 4-1: Scenarios used in BRAGFLO Salado flow modeling.

Scenario	Description
S1-BF	Undisturbed Repository
S2-BF	E1 intrusion at 350 years
S3-BF	E1 intrusion at 1,000 years
S4-BF	E2 intrusion at 350 years
S5-BF	E2 intrusion at 1,000 years

4.1.1 Scenario 1 (S1-DBR)

The BRAGFLO Salado modeling results from the S1-BF scenario are used as initial conditions in the computation of DBRs for the first intrusion into the repository. The S1-BF scenario represents an undisturbed repository (Camphouse, 2013b). In the computation of DBRs for this scenario, drilling intrusions at the upper, middle, and lower locations are modeled as occurring at intrusion times of 100, 350, 1,000, 3,000, 5,000, and 10,000 years (3 locations × 6 intrusion times × 100 vectors = 1,800 calculations per replicate).

Table 4-2: Intrusion times modeled by DBR for each scenario.

Scenario	Intrusion times (years)
S1-DBR	100, 350, 1000, 3000, 5000, 10000
S2-DBR	550, 750, 2000, 4000, 10000
S3-DBR	1200, 1400, 3000, 5000, 10000
S4-DBR	550, 750, 2000, 4000, 10000
S5-DBR	1200, 1400, 3000, 5000, 10000

4.1.2 Scenario 2 (S2-DBR)

BRAGFLO Salado flow modeling results from the scenario S2-BF are used as initial conditions for DBR calculations associated with a second or subsequent intrusion into the repository, where

the prior (E1) intrusion had intersected an underlying pressurized Castile brine reservoir at 350 years (Camphouse, 2013b). For the second or subsequent intrusion, drilling intrusions at upper, middle, and lower locations were modeled at 550, 750, 2,000, 4,000 and 10,000 years (3 locations \times 5 intrusion times \times 100 vectors = 1,500 calculations per replicate). The effect of the prior intrusion is incorporated in the calculations by specifying it as a boundary condition well, denoted by the red dot in Figure 3-1. The properties of the boundary condition well correspond to those at the time of the second intrusion.

Computations for the lower drilling location assume that the second or subsequent intrusion occurs at the location labeled “down-dip well” in Figure 3-1. It represents an intrusion in the same panel that was intersected by the prior intrusion (assumed to be at the location labeled “boundary condition well”). The previous intrusion or abandoned borehole is assumed to still connect the panel with the underlying brine reservoir. Model runs for the middle drilling location assume that the second or subsequent intrusion occurs at the location labeled “middle well” in Figure 3-1. As in the lower intrusion case, the prior intrusion is assumed to have occurred at the location labeled “boundary condition well.” For the middle intrusion however, the prior intrusion location is in an adjacent panel. Runs for the upper drilling location assume that the second or subsequent intrusion occurs at the location labeled “up-dip well” in Figure 3-1; a previous intrusion is assumed to have occurred at the location labeled “boundary condition well,” which is neither in the same panel nor in a panel adjacent to the current intrusion.

4.1.3 Scenario 3 (S3-DBR)

The BRAGFLO Salado modeling results from the S3-BF scenario are used as initial conditions for DBR calculations associated with a second or subsequent intrusion into the repository in which a prior intrusion had intersected an underlying pressurized Castile brine reservoir at 1,000 years (Camphouse, 2013b). Upper, middle, and lower second or subsequent intrusions are modeled at 1,200, 1,400, 3,000, 5,000 and 10,000 years (3 locations \times 5 intrusion times \times 100 vectors = 1,500 calculations per replicate). The effect of the prior E1 intrusion and the lower, middle, and upper drilling locations are treated the same as for the S2-DBR scenario.

4.1.4 Scenario 4 (S4-DBR)

For this scenario, the BRAGFLO Salado flow modeling results from the S4-BF scenario are used as initial conditions to compute DBRs for a second or subsequent intrusion into the repository, where a prior intrusion occurs at 350 years but does not intersect an underlying pressurized Castile brine reservoir (Camphouse, 2013b). Second or subsequent intrusions at the upper, middle, and lower locations are modeled as occurring at 550, 750, 2,000, 4,000 and 10,000 years (3 locations \times 5 intrusion times \times 100 vectors = 1,500 calculations per replicate). Runs for the lower drilling location assume the second or subsequent intrusion occurs at the location labeled “down-dip well” in Figure 3-1. This represents an intrusion into the same panel that was intersected by the prior E2 intrusion. The borehole from the previous intrusion is not represented explicitly in the model. Model runs for the middle drilling location assume that the second or subsequent intrusion occurs at the location labeled the “middle well” in Figures 3-1, whereas

those for the upper drilling location assume that the second or subsequent intrusion occurs at the location labeled “up-dip well” in Figure 3-1.

4.1.5 Scenario 5 (S5-DBR)

The BRAGFLO Salado flow modeling results from the scenario S5-BF are used as initial conditions in the computation of DBR volumes for the case of a second or subsequent intrusion into the repository, where the first intrusion occurs at 1,000 years without intersecting a Castile brine reservoir (Camphouse, 2013b). Upper, middle, and lower second or subsequent intrusions are modeled at 1,200, 1,400, 3,000, 5,000 and 10,000 years (3 locations × 5 intrusion times × 100 vectors = 1,500 calculations per replicate). The lower, middle, and upper drilling locations are treated the same as for the S4-DBR scenario.

4.2 Run Control

Run control, including code versions used and descriptions of code sequencing used to obtain DBR results in the CRA-2014 PA, are documented in Long (2013). The CRA-2014 PA initial conditions and results obtained from BRAGFLO DBR pre- and post-processing, respectively, are contained in files with the names:

1. ALG2_DBR_CRA14BL_Rr_Ss_Ttttt_Vvvv.CDB,
2. ALG3_DBR_CRA14BL_Rr_Ss_Ttttt_c_Vvvv.CDB,
3. ALG2_DBR_CRA14_Rr_Ss_Ttttt_Vvvv.CDB, and
4. ALG3_DBR_CRA14_Rr_Ss_Ttttt_c_Vvvv.CDB,

where r (the replicate number) equals 1,2, or 3, s (the scenario number) equals 1,2,3,4,5, or 6, tttt (time in years) equals 00550, 00750, 02000, 04000, or 10000, c (drilling location) is either L, M or U, and vvv (the vector number) is between 001 and 100. These files are located in CMS library LIBCRA14BL_DBRRrSs under class CRA14-BL, and LIBCRA14_DBRRrSs under class CRA14-0. PABC-2009 results used herein for purposes comparison have equivalent file names with ‘CRA14’ replaced by ‘PABC09’, and are located in CMS library LIBPABC09_DBRRrSs under class PABC09-0.

5 RESULTS

The DBR calculation results for the CRA-2014 PA are presented in this section and compared to results from the PABC-2009. The analysis of the PABC-2009 results is described in Clayton et al. (2010) and will only be summarized herein as appropriate. For consistency with previous analyses, non-zero volumes are defined as volumes that are greater than 10^{-7} m³. Given that only one replicate was executed for case CRA14-BL, the results for this case are compared to those of the PABC-2009 replicate 1. Case CRA14-0 results are assessed over all replicates and compared to those of all three replicates the PABC-2009.

As the case was for the PABC-2009, each replicate of DBR calculations in the CRA-2014 PA resulted in 7,800 separate vector-scenario-drilling location-time combinations (comprising 1,800 for first intrusion and $1,500 \times 4 = 6,000$ for second intrusion). These results are used as input to

the code CCDFGF, which then calculates a release for any vector-intrusion time combination. This is done by first, linearly interpolating modeled volumes between the fixed intrusion times (Table 4-2) and second, multiplying the resulting intrusion-specific DBR volume with the radionuclide concentration calculated for that vector and intrusion time by the code PANEL (Garner, 2010).

5.1 Summary

In this section, results of the BRAGFLO-DBR calculations for the CRA-2014 PA are compared to those of the PABC-2009. Pertinent summary statistics for the calculations are listed in Tables 5-1 and 5-2 for cases CRA14-BL and CRA14-0, respectively. As indicated above, the maximum DBR volumes shown in Table 5-1 are for replicate 1, whereas those shown in Table 5-2 are over all three replicates. The results for case CRA14-BL shown in Table 5-1 are consistent with those obtained in the 2012 panel closure system performance assessment (PCS-2012 PA) DBR calculations (Malama, 2012) with similar proportional increments in maximum DBR volumes compared to the PABC-2009 results. The results in Tables 5-1 and 5-2 are for all intrusion times, vectors and drilling locations.

Overall there is a consistent increase in the maximum DBR volumes from the PABC-2009 to the CRA-2014 PA (~10% for CRA14-BL and ~20% for CRA14-0). For case CRA14-BL, the largest increases were observed in scenarios S1-DBR and S5-DBR, with latter being comparable to the change in scenario S4-DBR. For case CRA14-0, where DBR volume maxima are computed over all three replicates, the largest increases were in scenarios S4-DBR and S5-DBR, which are associated with E2 intrusions. Implementing only the baseline changes (case CRA14-BL) as discussed above, yielded decreases in DBR volume maxima for scenarios S2-DBR and S3-DBR (see Table 5-1). The additional changes implemented in case CRA14-0 yielded increased DBR volume maxima (see Table 5-2), likely due to increased waste panel brine saturation seen for E1 intrusions in the Salado flow modeling results (Camphouse, 2013b).

For undisturbed repository conditions, implementation of the baseline changes discussed above (case CRA14-BL) yields a modest reduction in the mean waste panel pressure from the values computed in the PABC-2009 (Camphouse, 2013b). This reduction in pressure due to baseline changes is primarily attributable to an expansion in the mined volume. Updating the iron corrosion parameter leads to a reduced gas generation rate and a significant drop in mean waste panel pressure relative to the PABC-2009 (Camphouse, 2013b). The reduction in mean waste panel pressure for both cases CRA14-BL and CRA14-0 in turn leads to a higher pressure differential (or gradient) between the waste areas and the Salado formation. This has the effect of increasing the mean cumulative brine inflow into the waste areas in the CRA-2014 PA results compared to the PABC-2009. This increase in brine inflow eventually leads to higher waste panel brine saturation and higher maximum and average DBR volumes for scenario S1-DBR in the CRA-2014 than for the PABC-2009.

The BRAGFLO modeling results reported by Camphouse (2013b), show that, for a limited period of time after the intrusion, E1 intrusion scenarios (S2-BF and S3-BF) in the CRA-2014 PA yielded higher waste panel pressures, on average, than those observed in the PABC-2009 in the intruded panel. This increase in mean intruded panel pressure is due to the fact that the lower

long-term permeability range of the ROMPCS as compared to Option D yields a period of increased waste panel pressurization following an E1 intrusion. The mean intruded panel pressure computed in the CRA-2014 PA however, eventually decreases below that computed in the PABC-2009. This is primarily due to the slower gas production resulting from the revised iron corrosion rate. As for the undisturbed case, this decrease in intruded panel leads to a higher pressure differential (or gradient) between the intruded panel and the Salado formation as well as underlying Castile brine reservoir. It has the effect of increasing the overall cumulative brine inflows into the intruded panel. Increased brine inflows lead to increased mean brine saturation in the intruded panel. These factors explain the observed increases in the maximum DBR volumes from PABC-2009 to CRA-2014 PA, since DBRs are strongly dependent on waste panel pressure and brine saturation at the time of intrusion.

In a manner similar to the E1 intrusion scenarios results, changes included in the CRA-2014 PA since the PABC-2009 yield a decrease in the mean intruded panel pressure associated with E2 intrusion scenarios, S4-DBR and S5-DBR, due to the slower gas generation rate associated with the revised iron corrosion rate. The decreased panel pressures lead to increased brine inflows into the waste panel and to higher mean panel brine saturation. These factors explain the observed increases in the maximum DBR volumes from PABC-2009 to CRA-2014 PA, since DBRs are strongly dependent on waste panel pressure and brine saturation at the time of intrusion

Table 5-1: Summary statistics for case CRA-14BL and the PABC-2009 DBR calculations for replicate 1 over all vectors.

Scenario	Number of Vectors		Maximum volume (m ³)		Average volume (m ³)	
	PABC-2009	CRA14BL	PABC-2009	CRA14BL	PABC-2009	CRA14BL
S1-DBR	122	134	15.60	45.75	0.09	1.41
S2-DBR	388	386	41.80	37.23	2.88	3.89
S3-DBR	310	305	40.64	35.21	1.47	2.23
S4-DBR	74	89	19.30	38.73	0.05	0.48
S5-DBR	102	124	19.70	39.58	0.09	0.69
Overall	996	1038	41.80	45.75	0.92	1.74

Note: The volume of direct brine released was obtained from the output variable BRIN_REL which is calculated in the ALGEBRACDB step 3 post-processing step, and contained in the ALG3 CDB files.

Table 5-2: Summary statistics for the CRA-2014 PA and PABC-2009 DBR calculations for all replicates and all vectors.

Scenario	Number of Vectors		Maximum volume (m ³)		Average volume (m ³)	
	PABC-2009	CRA-2014 PA	PABC-2009	CRA-2014 PA	PABC-2009	CRA-2014 PA
S1-DBR	369	220	27.60	47.31	0.10	0.22
S2-DBR	1179	1140	48.20	58.02	2.80	3.78
S3-DBR	926	988	40.60	55.09	1.50	2.65
S4-DBR	211	104	20.40	36.77	0.10	0.15
S5-DBR	314	133	21.10	36.60	0.10	0.17
Overall	2999	2585	48.20	58.02	0.92	1.39

Note: The volume of direct brine released was obtained from the output variable BRIN_REL which is calculated in the ALGEBRACDB step 3 post-processing step, and contained in the ALG3 CDB files.

Information Only

5.2 Direct Brine Releases from the Lower Drilling Location

Tables 5-3 through 5-12 provide the summary statistics of the DBR volumes computed in the CRA-2014 PA. These statistics are (1) the number of vectors with non-zero DBR volumes, (2) the maximum and (3) average DBR volumes over all vectors in each scenario-time-drilling location combination. The corresponding summary statistics for the PABC-2009 are included in the tables for comparison. As already mentioned above, computations were undertaken for only one replicate in case CRA14-BL, and for three replicate in case CRA14-0. Tables 5-3, 5-5, 5-7, 5-9, and 5-11 give the summary statistics for comparison of case CRA14-BL and PABC-2009 results, while Tables 5-4, 5-6, 5-8, 5-10, and 5-12 give those for the CRA14-0 and PABC-2009 comparison. The results for case CRA14-BL are comparable to those of the PCS-2012 PA (Malama, 2012), with the differences between these two analyses being attributable to inclusion of an additional mined region in the north end of the repository, and update to waste inventory parameters.

One important conclusion that can be drawn from the results in Tables 5-3 through 5-12 is that DBRs are less likely to occur in intrusions situated in the up-dip (upper) drilling location than in the down-dip (lower) drilling location (Clayton, 2008; 2010). Of all the intrusions that had a non-zero DBR volume for case CRA14-BL (one replicate) of the CRA-2014 PA, 64.6% occurred during a lower drilling intrusion, a slight decrease from the value of 67.1% for PABC-2009. For case CRA14-0 (three replicates), which includes changes to the iron corrosion rate and refined water budget implementation, 82.4% occurred in the lower location, compared to 66.6% in PABC-2009, a significant increase. This change from the PABC-2009 results to the case CRA14-0 results may be attributable to the refinement of the water budget implementation to include MgO hydration, increased mined-out volume and revision of the iron corrosion rate. BRAGFLO modeling (Camphouse, 2013b) indicates that refined implementation of the water budget results in lower mean brine saturation in the South and North Rest-of-Repository (SRoR and NRoR) in the CRA-2014 computations than in the PABC-2009 due to water sequestration through MgO hydration. This results in a repository that is drier overall in the CRA-2014 than in the PABC-2009 (Camphouse, 2013b).

It should also be noted that, for case CRA14-0, of all the intrusions that had a non-zero DBR volume and occur during a down-dip (lower) drilling intrusion, 89.9% are found in scenarios S2-DBR and S3-DBR, a modest increase from 82.9% for PABC-2009 (Clayton et al., 2010). For case CRA14-BL, 78.8% are in scenarios S2-DBR and S3-DBR, a slight decrease from 82.3% for the PABC-2009. These results, as has been observed previously (Clayton et al., 2010; Pasch and Camphouse, 2011), simply show that the majority of the non-zero DBR volumes occur when there is a previous E1 intrusion within the same panel.

Not only are DBRs less likely to occur during a drilling intrusion in the up-dip (upper) location, but also the DBR volumes from such intrusions tend to be much smaller than those from lower drilling intrusions. For all three replicates of the CRA-2014 PA, the maximum DBR volume for the upper drilling location is 5.1 m³ compared to 58.0 m³ for the lower drilling location. These observations support the conclusion that lower drilling intrusions are the primary source for significant DBRs. The average DBR volumes are also consistently larger for the CRA-2014 PA than they were for the PABC-2009.

Table 5-3: Case CRA14-BL and PABC-2009 summary statistics of the DBR volumes for replicate 1 for the S1-DBR calculations.

Time (years)	Drilling Location	Number of Non-zero Vectors		Maximum volume (m ³)		Average volume (m ³)	
		PABC-2009	CRA14-BL	PABC-2009	CRA14-BL	PABC-2009	CRA14-BL
100	L	0	0	0.00E+00	0.00E+00	0.00E+00	0.00E+00
350	L	0	0	0.00E+00	0.00E+00	0.00E+00	0.00E+00
1,000	L	12	13	1.51E+01	4.26E+01	2.16E-01	2.36E+00
3,000	L	11	16	5.76E+00	3.81E+01	1.33E-01	3.09E+00
5,000	L	15	15	1.19E+01	4.57E+01	1.62E-01	5.13E+00
10,000	L	15	20	1.56E+01	4.50E+01	2.52E-01	4.79E+00
100	M	0	0	0.00E+00	0.00E+00	0.00E+00	0.00E+00
350	M	0	0	0.00E+00	0.00E+00	0.00E+00	0.00E+00
1,000	M	9	9	1.90E+00	3.78E+01	3.91E-02	5.76E-01
3,000	M	8	9	1.87E+00	1.41E+01	4.62E-02	2.40E-01
5,000	M	9	10	9.92E+00	1.10E+01	1.18E-01	2.82E-01
10,000	M	10	11	1.43E+00	1.06E+01	2.90E-02	1.96E-01
100	U	0	0	0.00E+00	5.53E-17	0.00E+00	0.00E+00
350	U	0	0	0.00E+00	4.49E-15	0.00E+00	0.00E+00
1,000	U	8	6	1.59E+00	2.98E+00	3.29E-02	3.52E-02
3,000	U	7	6	1.45E+00	1.71E+00	3.79E-02	3.18E-02
5,000	U	8	9	1.13E+00	1.17E+01	1.30E-02	1.21E-01
10,000	U	10	10	1.02E+00	1.54E+00	1.94E-02	1.94E-02

Note: All DBR volumes less than $1 \times 10^{-7} \text{ m}^3$ are set equal to 0.0 in this table. The maximum DBR volume is for 100 vectors for replicate 1 for each scenario-time-drilling location combination. The average DBR volume is calculated by the total of the DBR volumes divided by the total number of vectors. The DBR volume was obtained from the output variable BRIN_REL which is calculated in the ALGEBRACDB step 3 post-processing step, and contained in the ALG3 CDB files.

Information Only

Table 5-4: Case CRA14-0 and PABC-2009 summary statistics of the DBR volumes for all replicates for the S1-DBR calculations.

Time (years)	Drilling Location	Number of Non-zero Vectors		Maximum volume (m ³)		Average volume (m ³)	
		PABC-2009	CRA-2014 PA	PABC-2009	CRA-2014 PA	PABC-2009	CRA-2014 PA
100	L	0	0	0.00E+00	0.00E+00	0.00E+00	0.00E+00
350	L	0	0	0.00E+00	0.00E+00	0.00E+00	0.00E+00
1,000	L	26	0	1.51E+01	0.00E+00	1.80E-01	0.00E+00
3,000	L	37	25	5.92E+00	2.77E+01	1.16E-01	8.49E-01
5,000	L	46	43	2.19E+01	4.39E+01	2.92E-01	1.38E+00
10,000	L	46	52	2.03E+01	4.11E+01	4.26E-01	1.06E+00
100	M	0	0	0.00E+00	0.00E+00	0.00E+00	0.00E+00
350	M	0	0	0.00E+00	0.00E+00	0.00E+00	0.00E+00
1,000	M	19	0	6.33E+00	0.00E+00	5.14E-02	0.00E+00
3,000	M	32	13	2.27E+00	1.98E+01	3.95E-02	1.54E-01
5,000	M	29	22	2.25E+01	4.73E+01	1.24E-01	2.25E-01
10,000	M	31	23	2.76E+01	2.16E+01	1.32E-01	1.08E-01
100	U	0	0	0.00E+00	0.00E+00	0.00E+00	0.00E+00
350	U	0	0	0.00E+00	0.00E+00	0.00E+00	0.00E+00
1,000	U	16	0	6.15E+00	0.00E+00	4.75E-02	0.00E+00
3,000	U	29	15	1.73E+00	5.05E+00	3.13E-02	3.16E-02
5,000	U	28	23	2.02E+01	3.53E+00	7.82E-02	4.88E-02
10,000	U	30	28	1.91E+01	1.79E+00	9.37E-02	4.64E-02

Note: All DBR volumes less than $1 \times 10^{-7} \text{ m}^3$ are set equal to 0.0 in this table. The maximum DBR volume is for 300 vectors for 3 replicates for each scenario-time-drilling location combination. The average DBR volume is calculated by the total of the DBR volumes divided by the total number of vectors. The DBR volume was obtained from the output variable BRIN_REL which is calculated in the ALGEBRACDB step 3 post-processing step, and contained in the ALG3 CDB files.

Information Only

Table 5-5: Case CRA14-BL and PABC-2009 summary statistics of the DBR volumes for replicate 1 for the S2-DBR calculations.

Time (years)	Drilling Location	Number of Non-zero Vectors		Maximum volume (m ³)		Average volume (m ³)	
		PABC-2009	CRA14-BL	PABC-2009	CRA14-BL	PABC-2009	CRA14-BL
550	L	96	98	3.61E+01	3.67E+01	1.22E+01	1.26E+01
750	L	86	84	3.23E+01	3.51E+01	1.15E+01	1.36E+01
2,000	L	52	54	3.31E+01	3.52E+01	7.44E+00	1.16E+01
4,000	L	43	41	3.85E+01	3.58E+01	5.46E+00	9.63E+00
10,000	L	46	41	4.18E+01	3.72E+01	5.89E+00	9.37E+00
550	M	4	3	4.41E+00	9.87E+00	5.12E-02	1.24E-01
750	M	7	7	2.23E+00	2.60E+01	3.20E-02	2.82E-01
2,000	M	10	12	7.01E+00	3.17E+01	1.83E-01	5.22E-01
4,000	M	9	9	2.10E+01	1.19E+01	2.47E-01	2.45E-01
10,000	M	7	12	1.82E+00	1.83E+01	3.49E-02	3.14E-01
550	U	3	1	4.14E-01	3.48E-02	5.70E-03	3.48E-04
750	U	4	3	2.35E+00	1.32E-01	2.48E-02	1.41E-03
2,000	U	8	6	6.85E+00	7.66E+00	1.50E-01	9.75E-02
4,000	U	7	6	1.12E+00	3.60E-01	1.93E-02	9.41E-03
10,000	U	6	9	1.01E+00	1.46E+00	2.50E-02	1.92E-02

Note: All DBR volumes less than $1 \times 10^{-7} \text{ m}^3$ are set equal to 0.0 in this table. The maximum DBR volume is for 100 vectors for replicate 1 for each scenario-time-drilling location combination. The average DBR volume is calculated by the total of the DBR volumes divided by the total number of vectors. The DBR volume was obtained from the output variable BRIN_REL which is calculated in the ALGEBRACDB step 3 post-processing step, and contained in the ALG3 CDB files.

Information Only

Table 5-6: Case CRA14-0 and PABC-2009 summary statistics of the DBR volumes for all replicates for the S2-DBR calculations.

Time (years)	Drilling Location	Number of Non-zero Vectors		Maximum volume (m ³)		Average volume (m ³)	
		PABC-2009	CRA-2014 PA	PABC-2009	CRA-2014 PA	PABC-2009	CRA-2014 PA
550	L	285	281	3.74E+01	3.28E+01	1.23E+01	1.13E+01
750	L	255	286	3.86E+01	3.78E+01	1.16E+01	1.36E+01
2,000	L	164	215	3.78E+01	4.27E+01	7.11E+00	1.28E+01
4,000	L	140	165	4.39E+01	4.64E+01	5.38E+00	1.10E+01
10,000	L	137	102	4.82E+01	5.80E+01	5.64E+00	7.41E+00
550	M	7	0	4.41E+00	2.25E-14	1.71E-02	2.81E-16
750	M	15	0	7.63E+00	2.98E-14	5.02E-02	3.13E-16
2,000	M	32	5	8.70E+00	1.89E+01	1.42E-01	8.38E-02
4,000	M	30	23	2.10E+01	2.95E+01	9.88E-02	2.49E-01
10,000	M	24	26	1.79E+01	2.63E+01	1.25E-01	1.38E-01
550	U	5	0	4.14E-01	2.82E-16	1.91E-03	2.30E-18
750	U	9	0	2.35E+00	5.26E-16	9.01E-03	3.18E-18
2,000	U	27	1	9.68E+00	2.21E+00	1.12E-01	7.38E-03
4,000	U	27	15	1.18E+00	4.55E+00	1.54E-02	5.65E-02
10,000	U	22	21	1.24E+01	1.35E+00	7.96E-02	3.79E-02

Note: All DBR volumes less than $1 \times 10^{-7} \text{ m}^3$ are set equal to 0.0 in this table. The maximum DBR volume is for 300 vectors for 3 replicates for each scenario-time-drilling location combination. The average DBR volume is calculated by the total of the DBR volumes divided by the total number of vectors. The DBR volume was obtained from the output variable BRIN_REL which is calculated in the ALGEBRACDB step 3 post-processing step, and contained in the ALG3 CDB files.

Information Only

Table 5-7: Case CRA14-BL and PABC-2009 summary statistics of the DBR volumes for replicate 1 for the S3-DBR calculations.

Time (years)	Drilling Location	Number of Non-zero Vectors		Maximum volume (m ³)		Average volume (m ³)	
		PABC-2009	CRA14-BL	PABC-2009	CRA14-BL	PABC-2009	CRA14-BL
1,200	L	78	79	3.32E+01	3.19E+01	8.31E+00	9.21E+00
1,400	L	54	54	2.18E+01	2.36E+01	4.91E+00	7.90E+00
3,000	L	34	31	2.25E+01	2.25E+01	2.50E+00	4.90E+00
5,000	L	30	24	3.76E+01	3.01E+01	3.05E+00	4.83E+00
10,000	L	31	23	4.06E+01	2.86E+01	2.53E+00	4.43E+00
1,200	M	10	11	1.81E+01	3.52E+01	1.93E-01	5.18E-01
1,400	M	13	13	1.40E+01	2.09E+01	2.63E-01	5.43E-01
3,000	M	7	9	3.59E+00	1.42E+01	7.33E-02	2.75E-01
5,000	M	9	9	1.07E+01	1.26E+01	1.32E-01	3.35E-01
10,000	M	7	12	1.48E+00	1.71E+01	2.63E-02	3.00E-01
1,200	U	9	10	5.32E-01	1.16E+00	9.48E-03	1.45E-02
1,400	U	8	7	1.21E-01	3.11E-01	2.45E-03	3.72E-03
3,000	U	8	7	1.95E+00	1.72E+00	4.59E-02	3.24E-02
5,000	U	7	7	1.08E+00	1.11E+01	1.49E-02	1.16E-01
10,000	U	5	9	1.02E+00	1.47E+00	2.04E-02	1.96E-02

Note: All DBR volumes less than $1 \times 10^{-7} \text{ m}^3$ are set equal to 0.0 in this table. The maximum DBR volume is for 100 vectors for replicate 1 for each scenario-time-drilling location combination. The average DBR volume is calculated by the total of the DBR volumes divided by the total number of vectors. The DBR volume was obtained from the output variable BRIN_REL which is calculated in the ALGEBRACDB step 3 post-processing step, and contained in the ALG3 CDB files.

Information Only

Table 5-8: Case CRA14-0 and PABC-2009 summary statistics of the DBR volumes for all replicates for the S3-DBR calculations.

Time (years)	Drilling Location	Number of Non-zero Vectors		Maximum volume (m ³)		Average volume (m ³)	
		PABC-2009	CRA-2014 PA	PABC-2009	CRA-2014 PA	PABC-2009	CRA-2014 PA
1,200	L	231	285	3.68E+01	3.08E+01	8.76E+00	1.02E+01
1,400	L	166	257	3.25E+01	2.82E+01	5.41E+00	8.21E+00
3,000	L	96	157	2.68E+01	3.55E+01	2.47E+00	7.27E+00
5,000	L	90	110	3.76E+01	4.69E+01	2.70E+00	7.23E+00
10,000	L	90	75	4.06E+01	5.51E+01	2.76E+00	6.17E+00
1,200	M	27	0	1.81E+01	1.78E-14	1.58E-01	2.76E-16
1,400	M	32	0	1.98E+01	1.39E-14	2.13E-01	2.63E-16
3,000	M	29	13	3.59E+00	1.59E+01	4.48E-02	1.33E-01
5,000	M	26	25	2.17E+01	3.77E+01	1.21E-01	2.46E-01
10,000	M	21	25	1.34E+01	2.64E+01	6.40E-02	1.40E-01
1,200	U	23	0	4.39E+00	5.52E-16	4.45E-02	3.87E-18
1,400	U	23	0	2.64E+00	5.05E-16	3.60E-02	3.86E-18
3,000	U	29	4	1.95E+00	4.72E+00	3.39E-02	2.97E-02
5,000	U	24	16	1.96E+01	2.97E+00	7.33E-02	4.97E-02
10,000	U	19	21	1.22E+01	1.34E+00	7.35E-02	3.66E-02

Note: All DBR volumes less than $1 \times 10^{-7} \text{ m}^3$ are set equal to 0.0 in this table. The maximum DBR volume is for 300 vectors for 3 replicates for each scenario-time-drilling location combination. The average DBR volume is calculated by the total of the DBR volumes divided by the total number of vectors. The DBR volume was obtained from the output variable BRIN_REL which is calculated in the ALGEBRACDB step 3 post-processing step, and contained in the ALG3 CDB files.

Information Only

Table 5-9: Case CRA14-BL and PABC-2009 summary statistics of the DBR volumes for replicate 1 for the S4-DBR calculations.

Time (years)	Drilling Location	Number of Non-zero Vectors		Maximum volume (m ³)		Average volume (m ³)	
		PABC-2009	CRA14-BL	PABC-2009	CRA14-BL	PABC-2009	CRA14-BL
550	L	3	4	1.00E+00	3.22E+01	1.21E-02	1.51E+00
750	L	2	3	1.93E+01	9.24E+00	1.93E-01	3.47E-01
2,000	L	6	8	7.34E+00	1.80E+01	7.56E-02	5.74E-01
4,000	L	8	10	2.03E+00	3.81E+01	2.12E-02	1.60E+00
10,000	L	8	8	1.28E+01	3.87E+01	1.62E-01	1.56E+00
550	M	3	3	5.48E-01	8.05E+00	7.32E-03	1.08E-01
750	M	5	5	2.61E+00	2.36E+01	2.97E-02	2.55E-01
2,000	M	4	9	5.17E+00	3.08E+01	6.12E-02	5.00E-01
4,000	M	6	8	1.72E+00	1.26E+01	3.51E-02	2.49E-01
10,000	M	5	8	1.48E+00	2.04E+01	2.11E-02	3.33E-01
550	U	3	1	4.12E-01	3.45E-02	5.64E-03	3.45E-04
750	U	4	3	2.05E+00	1.23E-01	2.17E-02	1.34E-03
2,000	U	6	5	7.68E+00	7.58E+00	1.25E-01	9.66E-02
4,000	U	6	7	1.21E+00	4.31E-01	2.06E-02	1.09E-02
10,000	U	5	7	1.06E+00	1.48E+00	1.94E-02	2.04E-02

Note: All DBR volumes less than $1 \times 10^{-7} \text{ m}^3$ are set equal to 0.0 in this table. The maximum DBR volume is for 100 vectors for replicate 1 for each scenario-time-drilling location combination. The average DBR volume is calculated by the total of the DBR volumes divided by the total number of vectors. The DBR volume was obtained from the output variable BRIN_REL which is calculated in the ALGEBRACDB step 3 post-processing step, and contained in the ALG3 CDB files.

Information Only

Table 5-10: Case CRA14-0 and PABC-2009 summary statistics of the DBR volumes for all replicates for the S4-DBR calculations.

Time (years)	Drilling Location	Number of Non-zero Vectors		Maximum volume (m ³)		Average volume (m ³)	
		PABC-2009	CRA-2014 PA	PABC-2009	CRA-2014 PA	PABC-2009	CRA-2014 PA
550	L	6	0	1.00E+00	2.55E-14	4.09E-03	5.60E-16
750	L	5	0	1.93E+01	1.27E-14	7.36E-02	5.23E-16
2,000	L	17	4	1.60E+01	8.97E+00	1.44E-01	1.96E-01
4,000	L	22	14	1.92E+01	3.68E+01	9.43E-02	5.72E-01
10,000	L	24	22	2.04E+01	2.91E+01	2.11E-01	9.50E-01
550	M	6	0	5.48E-01	2.18E-14	2.47E-03	2.81E-16
750	M	9	0	2.61E+00	2.50E-14	1.08E-02	2.96E-16
2,000	M	18	4	8.25E+00	1.62E+01	7.98E-02	6.98E-02
4,000	M	19	15	1.72E+00	2.31E+01	2.00E-02	1.71E-01
10,000	M	14	16	1.48E+00	2.64E+01	9.71E-03	1.41E-01
550	U	5	0	4.12E-01	2.89E-16	1.89E-03	2.46E-18
750	U	8	0	2.05E+00	4.40E-16	7.93E-03	3.55E-18
2,000	U	22	1	9.60E+00	2.06E+00	1.05E-01	6.86E-03
4,000	U	21	11	1.21E+00	3.94E+00	1.26E-02	4.11E-02
10,000	U	15	17	1.11E+01	1.29E+00	5.08E-02	2.91E-02

Note: All DBR volumes less than $1 \times 10^{-7} \text{ m}^3$ are set equal to 0.0 in this table. The maximum DBR volume is for 300 vectors for 3 replicates for each scenario-time-drilling location combination. The average DBR volume is calculated by the total of the DBR volumes divided by the total number of vectors. The DBR volume was obtained from the output variable BRIN_REL which is calculated in the ALGEBRACDB step 3 post-processing step, and contained in the ALG3 CDB files.

Information Only

Table 5-11: Case CRA14-BL and PABC-2009 summary statistics of the DBR volumes for replicate 1 for the S5-DBR calculations.

Time (years)	Drilling Location	Number of Non-zero Vectors		Maximum volume (m ³)		Average volume (m ³)	
		PABC-2009	CRA14-BL	PABC-2009	CRA14-BL	PABC-2009	CRA14-BL
1,200	L	12	15	1.97E+01	3.96E+01	3.77E-01	2.94E+00
1,400	L	5	5	1.27E+01	1.63E+01	1.73E-01	8.43E-01
3,000	L	6	10	3.04E+00	3.66E+01	3.05E-02	1.27E+00
5,000	L	7	7	1.86E+00	3.75E+01	2.44E-02	1.72E+00
10,000	L	8	8	1.28E+01	3.85E+01	1.66E-01	1.55E+00
1,200	M	9	11	1.81E+01	3.55E+01	1.94E-01	5.22E-01
1,400	M	9	9	1.39E+01	2.00E+01	2.52E-01	3.84E-01
3,000	M	5	8	4.17E+00	1.42E+01	6.30E-02	2.72E-01
5,000	M	6	8	1.58E+00	1.33E+01	2.44E-02	3.49E-01
10,000	M	5	8	1.48E+00	1.93E+01	2.25E-02	3.23E-01
1,200	U	9	9	5.37E-01	1.17E+00	1.02E-02	1.45E-02
1,400	U	6	6	1.27E-01	3.36E-01	2.98E-03	3.94E-03
3,000	U	5	5	2.03E+00	1.67E+00	3.68E-02	3.26E-02
5,000	U	5	8	1.15E+00	1.07E+01	1.45E-02	1.12E-01
10,000	U	5	7	1.06E+00	1.49E+00	1.84E-02	2.05E-02

Note: All DBR volumes less than $1 \times 10^{-7} \text{ m}^3$ are set equal to 0.0 in this table. The maximum DBR volume is for 100 vectors for replicate 1 for each scenario-time-drilling location combination. The average DBR volume is calculated by the total of the DBR volumes divided by the total number of vectors. The DBR volume was obtained from the output variable BRIN_REL which is calculated in the ALGEBRACDB step 3 post-processing step, and contained in the ALG3 CDB files.

Information Only

Table 5-12: Case CRA14-0 and PABC-2009 summary statistics of the DBR volumes for all replicates for the S5-DBR calculations.

Time (years)	Drilling Location	Number of Non-zero Vectors		Maximum volume (m ³)		Average volume (m ³)	
		PABC-2009	CRA-2014 PA	PABC-2009	CRA-2014 PA	PABC-2009	CRA-2014 PA
1,200	L	31	1	1.97E+01	3.88E+00	3.17E-01	4.17E-02
1,400	L	15	2	2.11E+01	4.50E+00	2.05E-01	5.58E-02
3,000	L	18	12	6.01E+00	1.45E+01	6.79E-02	4.42E-01
5,000	L	23	19	9.25E+00	2.49E+01	6.25E-02	5.03E-01
10,000	L	24	24	2.03E+01	2.90E+01	2.10E-01	9.43E-01
1,200	M	25	0	1.81E+01	1.95E-14	1.53E-01	2.84E-16
1,400	M	26	0	1.98E+01	1.66E-14	2.11E-01	2.81E-16
3,000	M	21	9	4.17E+00	1.43E+01	4.01E-02	1.21E-01
5,000	M	19	15	1.58E+00	3.66E+01	1.28E-02	1.96E-01
10,000	M	14	16	1.48E+00	2.64E+01	1.02E-02	1.41E-01
1,200	U	21	0	4.32E+00	5.57E-16	3.56E-02	4.01E-18
1,400	U	20	0	2.67E+00	5.62E-16	3.81E-02	4.20E-18
3,000	U	23	4	2.03E+00	4.82E+00	3.13E-02	2.91E-02
5,000	U	19	13	1.15E+00	2.91E+00	7.91E-03	4.24E-02
10,000	U	15	18	1.11E+01	1.29E+00	5.03E-02	2.93E-02

Note: All DBR volumes less than $1 \times 10^{-7} \text{ m}^3$ are set equal to 0.0 in this table. The maximum DBR volume is for 300 vectors for 3 replicates for each scenario-time-drilling location combination. The average DBR volume is calculated by the total of the DBR volumes divided by the total number of vectors. The DBR volume was obtained from the output variable BRIN_REL which is calculated in the ALGEBRACDB step 3 post-processing step, and contained in the ALG3 CDB files.

Information Only

Figures 5-1 to 5-20 are probability plots of the DBR volumes for scenarios S1-DBR to S5-DBR for one replicate in case CRA14-BL and all three replicates for case CRA14-0. Results of the CRA-2014 PA are compared to those of the PABC-2009. The probability plots show the percentiles (x-axis) of the DBR volumes (y-axis). The plots of the case CRA14-BL results are in Figures 5-1, 5-5, 5-9, 5-13, and 5-17, whereas those from case CRA14-0 are in Figures 5-3, 5-7, 5-11, 5-15, and 5-19. The other figures are plots of the PABC-2009 results that are included for comparison.

The CRA-2014 results show appreciable changes in frequencies from the CRA-2014 PA to the PABC-2009. The results of case CRA14-BL are similar to those obtained in the PCS-2012 PA (Malama, 2012). Hence, the differences between the CRA14-BL and PABC-2009 results are primarily due to the implementation of the new panel closure system, ROMPCS. For the CRA-2014 PA results, as the case was for the PABC-2009, the largest DBR volume and the greatest probability of a non-zero volume occur in scenario S2-DBR. For all DBR volumes smaller than the maximum, the probability of occurrence of DBR volumes less than a given DBR volume is generally smaller in the CRA-2014 PA results than in the PABC-2009 at all intrusion times. This result implies that CRA-2014 PA DBR volumes are larger but less likely to occur compared to those of the PABC-2009.

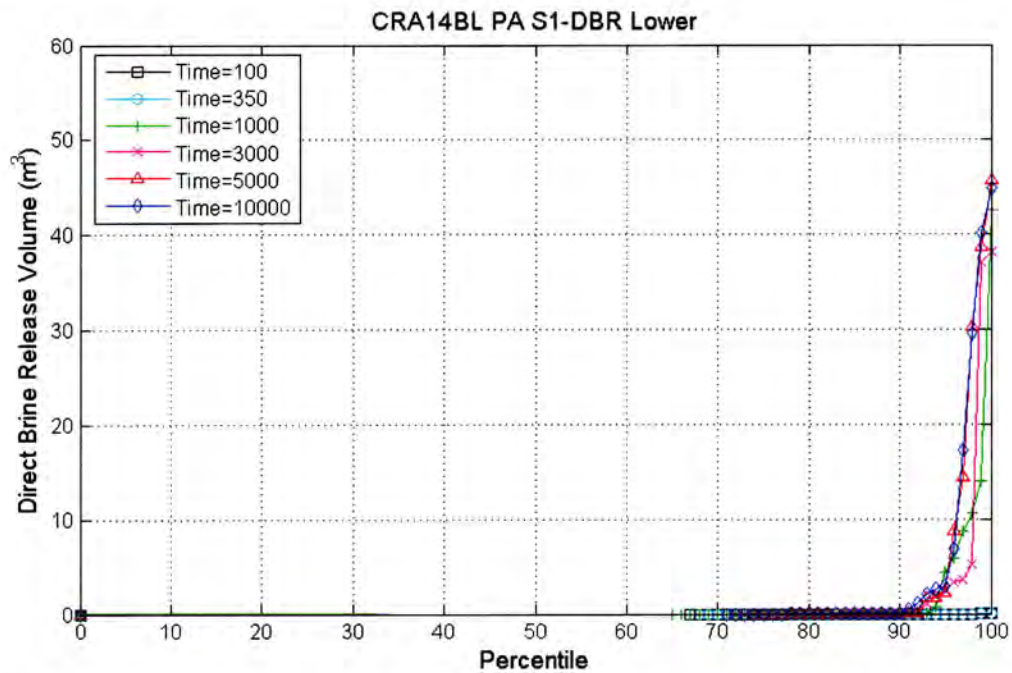


Figure 5-1: Plot of the percentile (x-axis) of DBR volumes that are less than the DBR volume on the y-axis for case CRA14-BL of the CRA-2014 PA at the lower intrusion location for replicate 1; scenario S1-DBR.

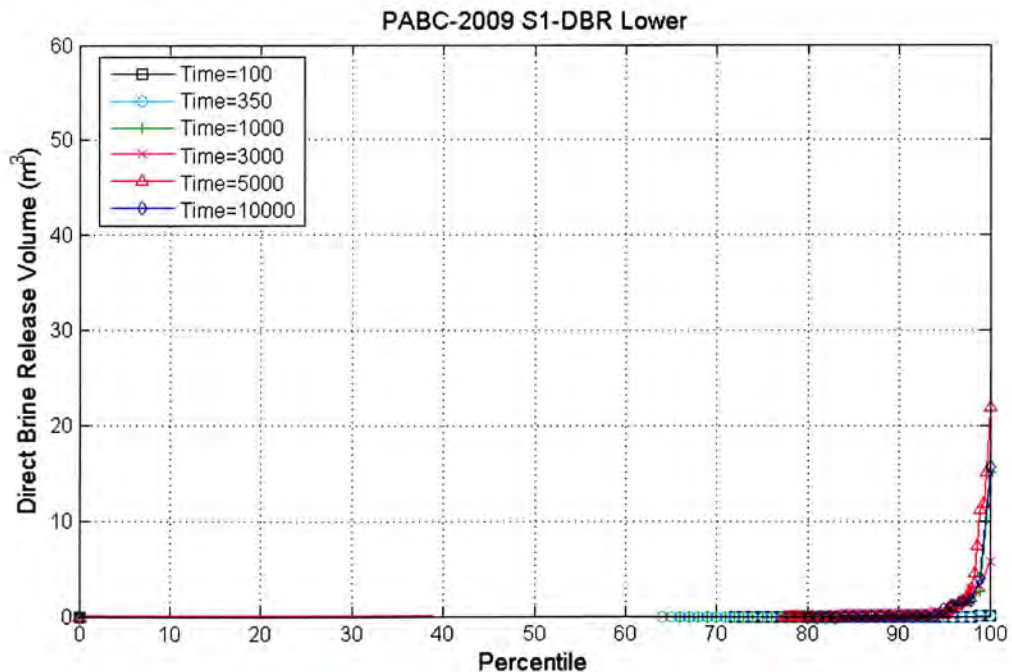


Figure 5-2: Plot of the percentile (x-axis) of DBR volumes that are less than the DBR volume on the y-axis for the PABC-2009 at the lower intrusion location for replicate 1; scenario S1-DBR.

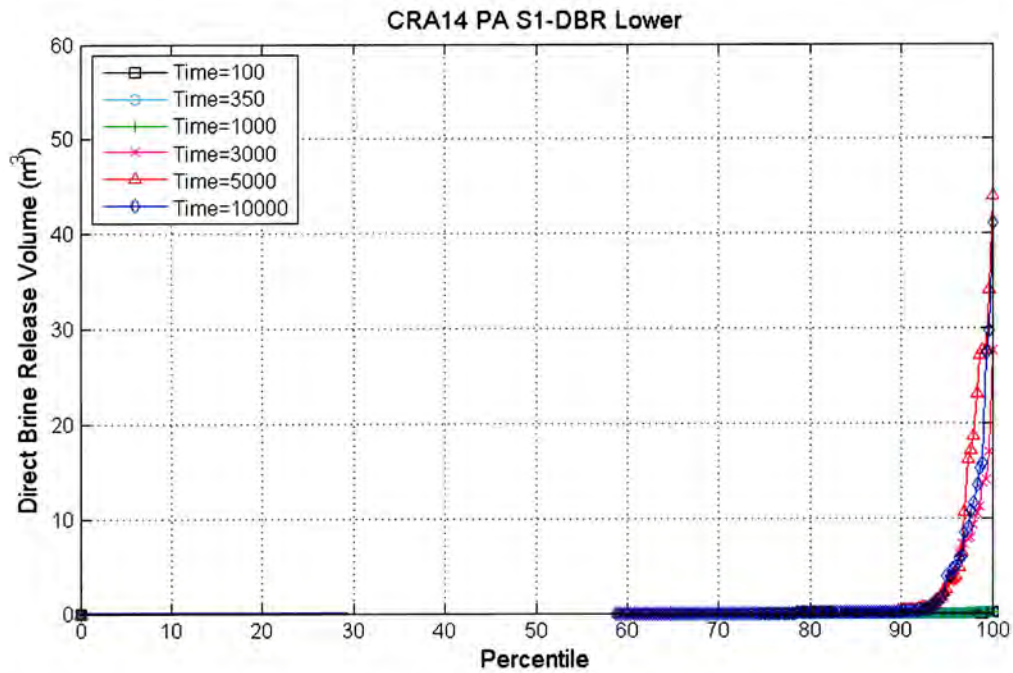


Figure 5-3: Plot of the percentile (x-axis) of DBR volumes that are less than the DBR volume on the y-axis for case CRA14-0 of the CRA-2014 PA at the lower intrusion location over all replicates; scenario S1-DBR.

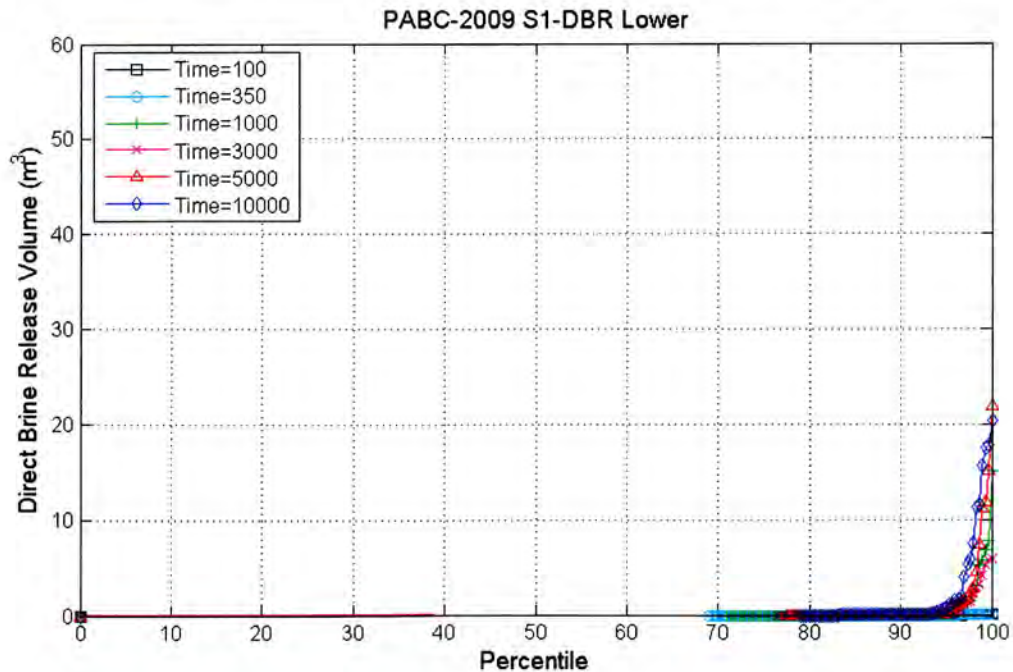


Figure 5-4: Plot of the percentile (x-axis) of DBR volumes that are less than the DBR volume on the y-axis for the PABC-2009 at the lower intrusion location for all replicates; scenario S1-DBR.

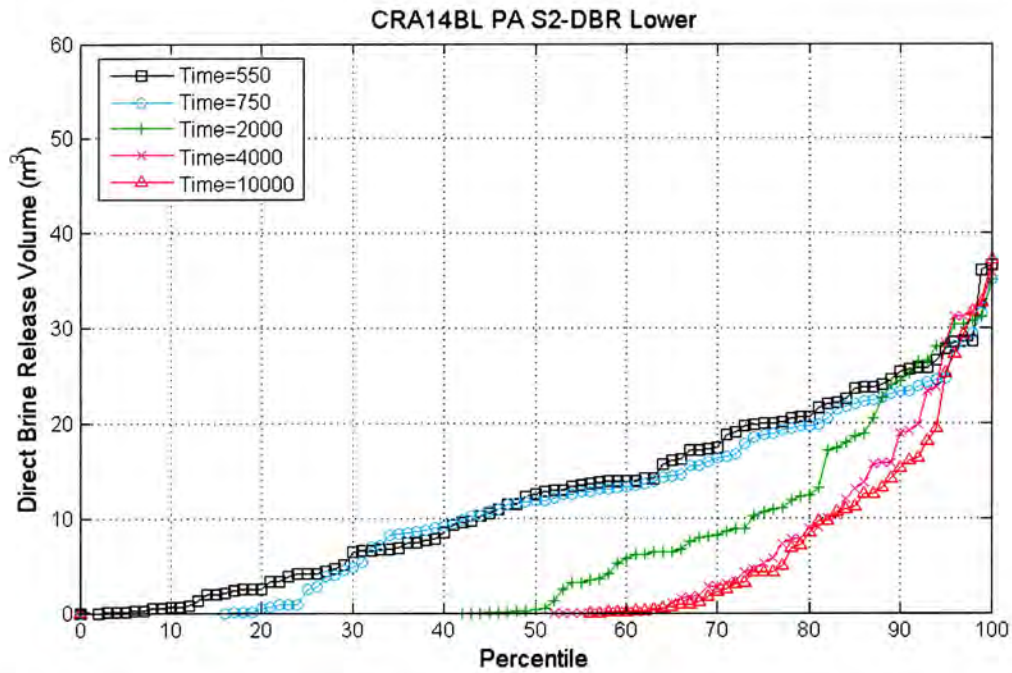


Figure 5-5: Plot of the percentile (x-axis) of DBR volumes that are less than the DBR volume on the y-axis for case CRA14-BL of the CRA-2014 PA at the lower intrusion location for replicate 1; scenario S2-DBR.

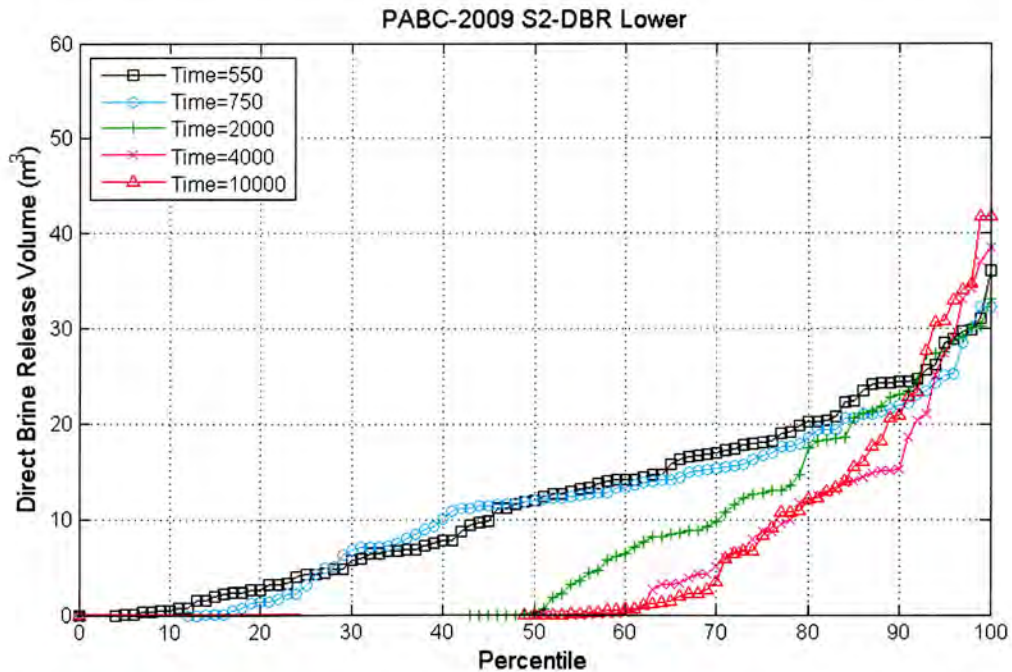


Figure 5-6: Plot of the percentile (x-axis) of DBR volumes that are less than the DBR volume on the y-axis for the PABC-2009 at the lower intrusion location for replicate 1; scenario S2-DBR.

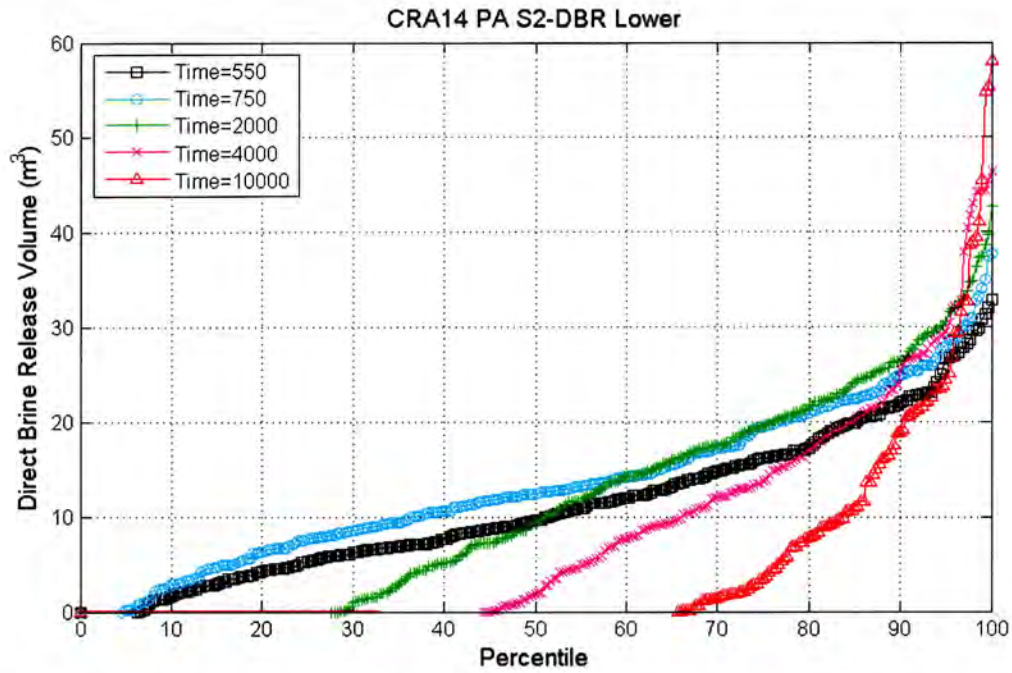


Figure 5-7: Plot of the percentile (x-axis) of DBR volumes that are less than the DBR volume on the y-axis for case CRA14-0 of the CRA-2014 PA at the lower intrusion location for all replicates; scenario S2-DBR.

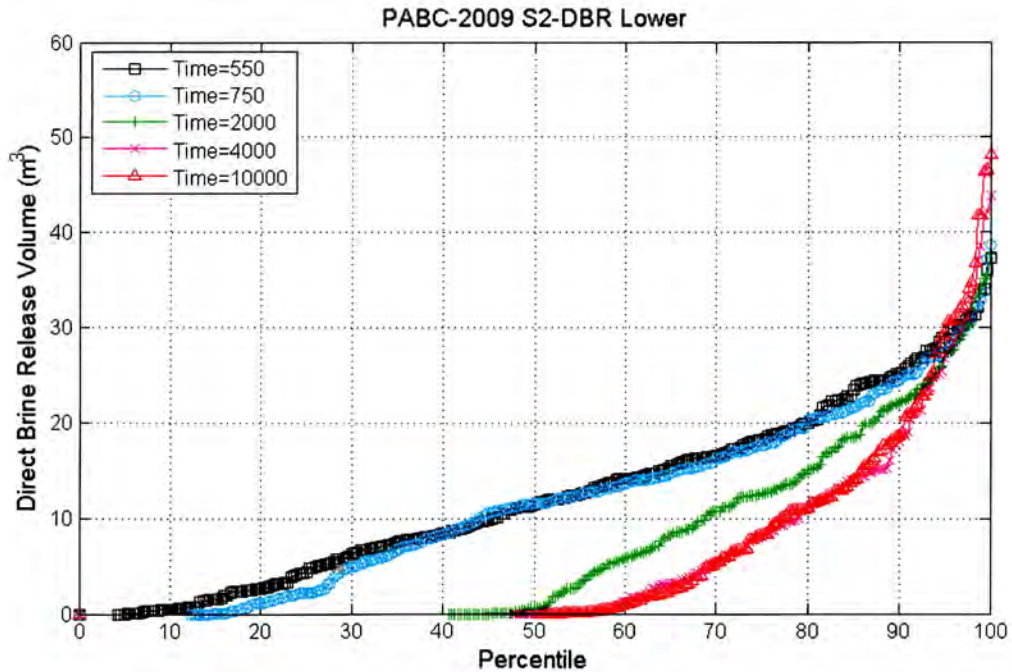


Figure 5-8: Plot of the percentile (x-axis) of DBR volumes that are less than the DBR volume on the y-axis for the PABC-2009 at the lower intrusion location for all replicates; scenario S2-DBR.

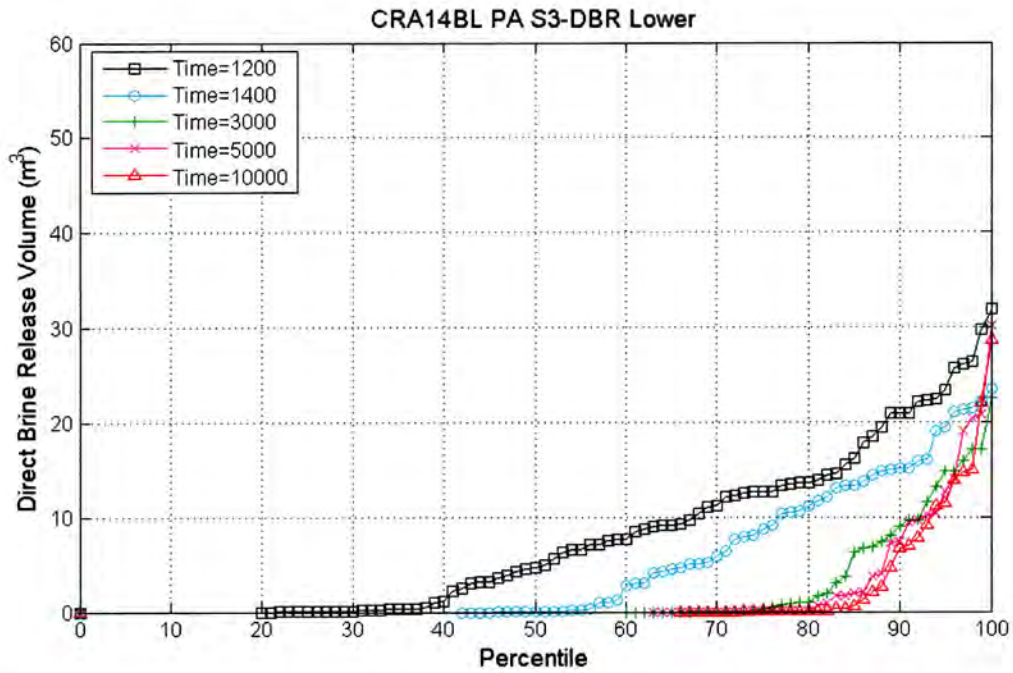


Figure 5-9: Plot of the percentile (x-axis) of DBR volumes that are less than the DBR volume on the y-axis for case CRA14-BL of the CRA-2014 PA at the lower intrusion location for replicate 1; scenario S3-DBR.

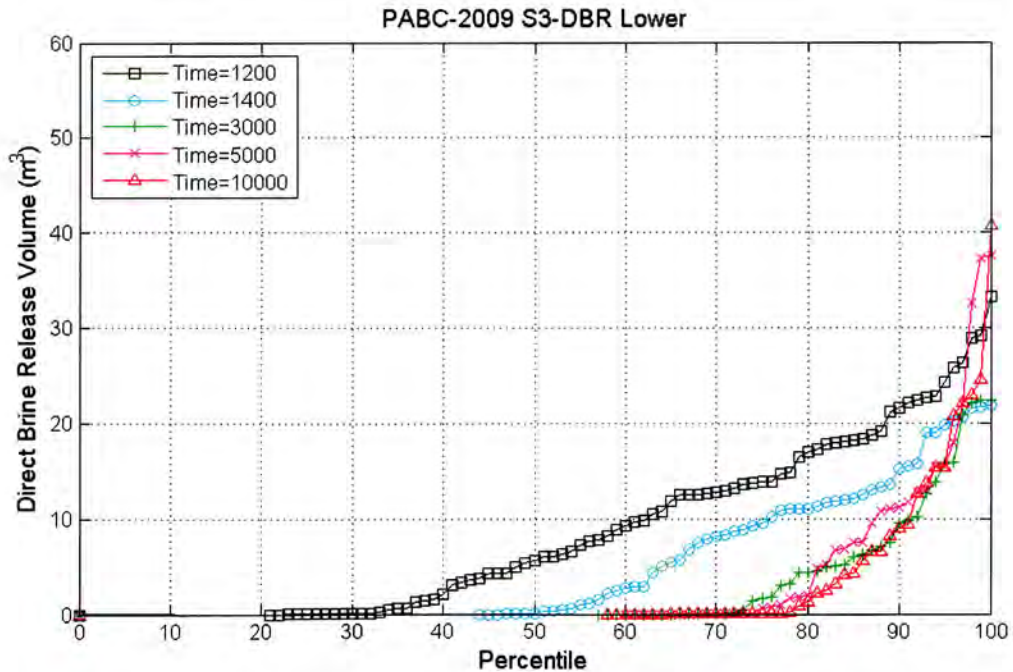


Figure 5-10: Plot of the percentile (x-axis) of DBR volumes that are less than the DBR volume on the y-axis for the PABC-2009 at the lower intrusion location for replicate 1; scenario S3-DBR.

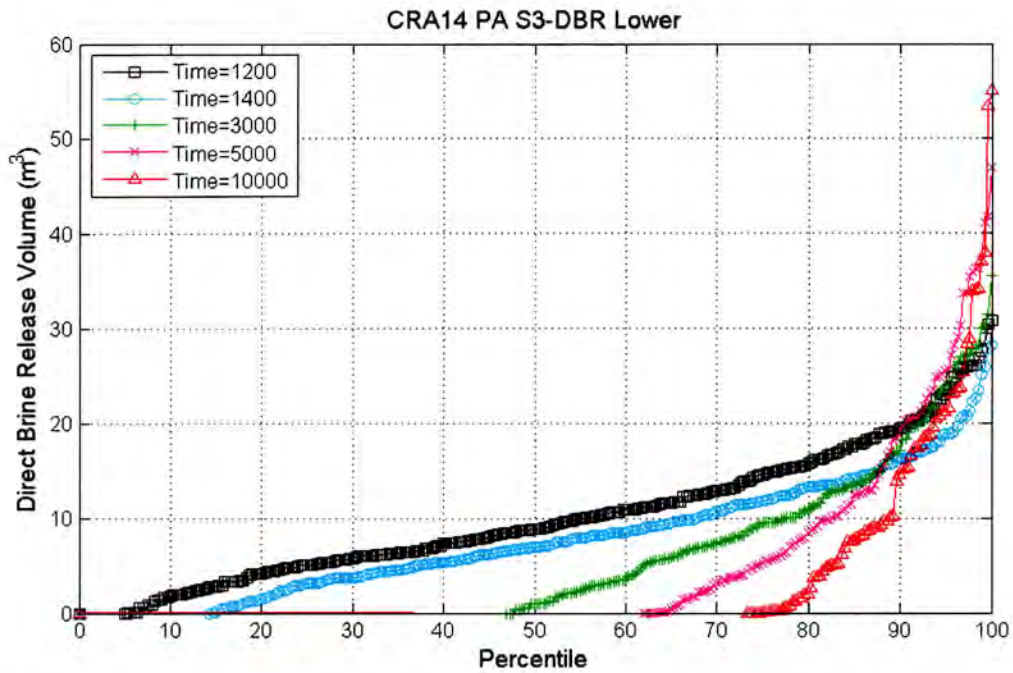


Figure 5-11: Plot of the percentile (x-axis) of DBR volumes that are less than the DBR volume on the y-axis for case CRA14-0 of the CRA-2014 PA at the lower intrusion location for all replicates; scenario S3-DBR.

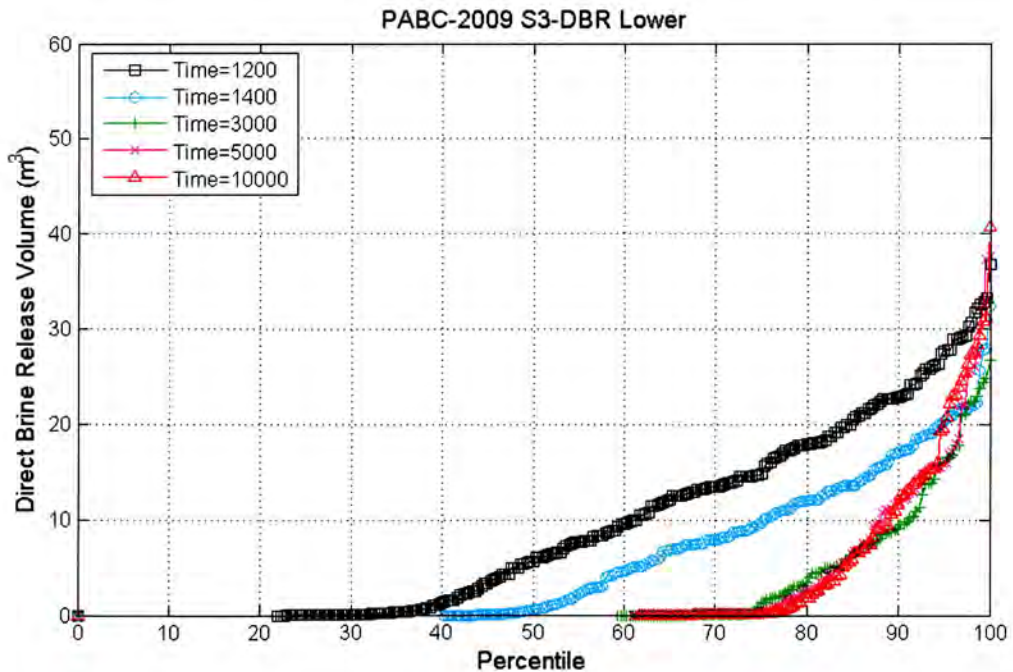


Figure 5-12: Plot of the percentile (x-axis) of DBR volumes that are less than the DBR volume on the y-axis for the PABC-2009 at the lower intrusion location for all replicates; scenario S3-DBR.

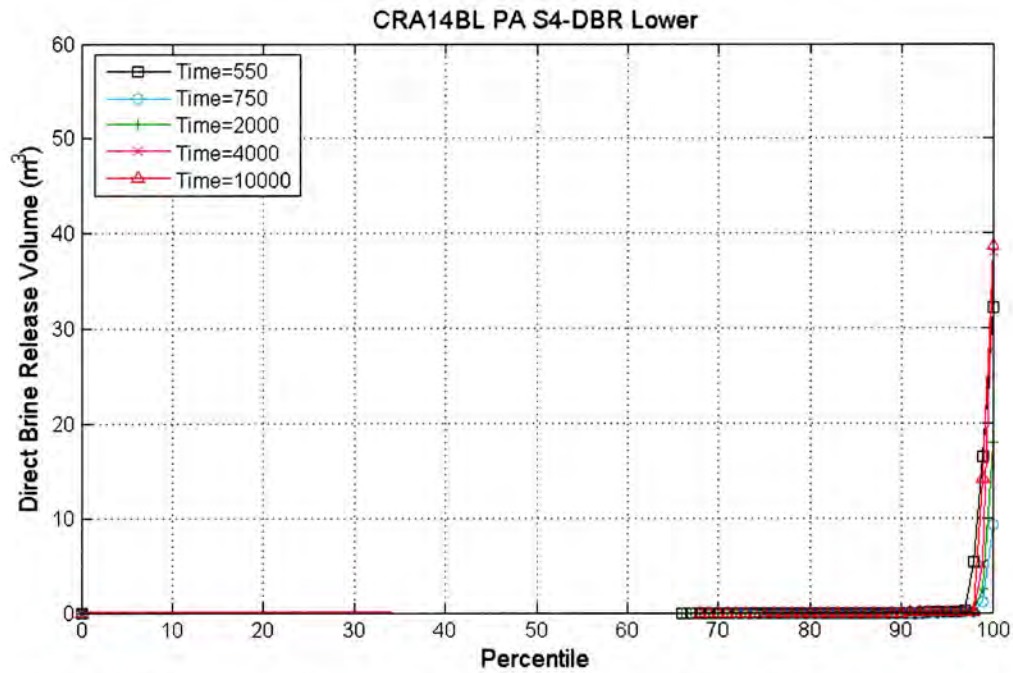


Figure 5-13: Plot of the percentile (x-axis) of DBR volumes that are less than the DBR volume on the y-axis for case CRA14-BL of the CRA-2014 PA at the lower intrusion location for replicate 1; scenario S4-DBR.

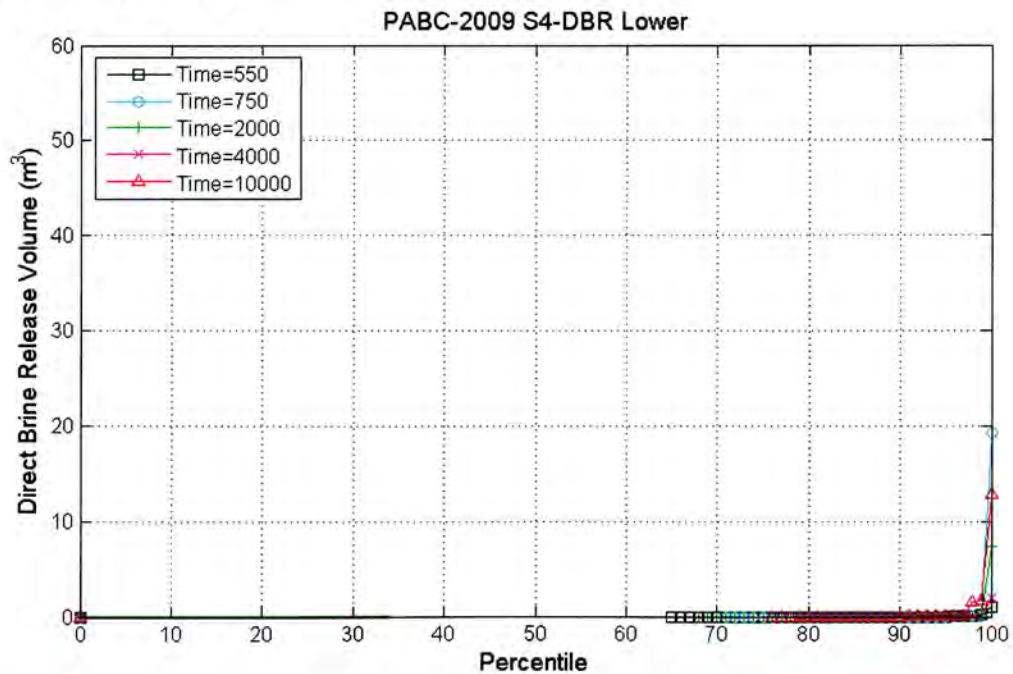


Figure 5-14: Plot of the percentile (x-axis) of DBR volumes that are less than the DBR volume on the y-axis for the PABC-2009 at the lower intrusion location for replicate 1; scenario S4-DBR.

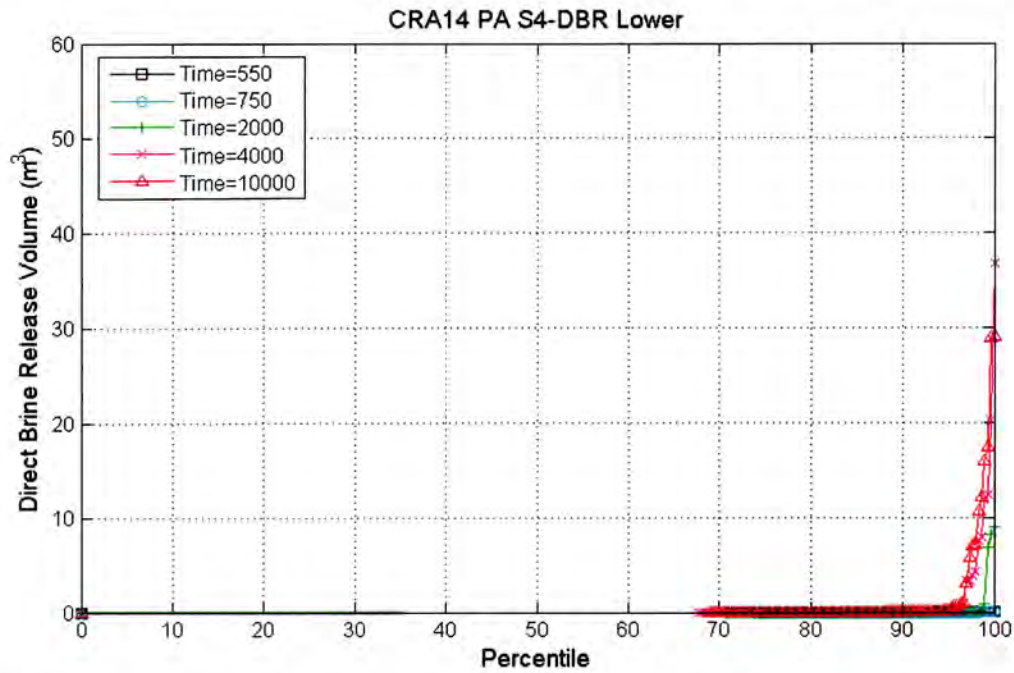


Figure 5-15: Plot of the percentile (x-axis) of DBR volumes that are less than the DBR volume on the y-axis for case CRA14-0 of the CRA-2014 PA at the lower intrusion location for all replicates; scenario S4-DBR.

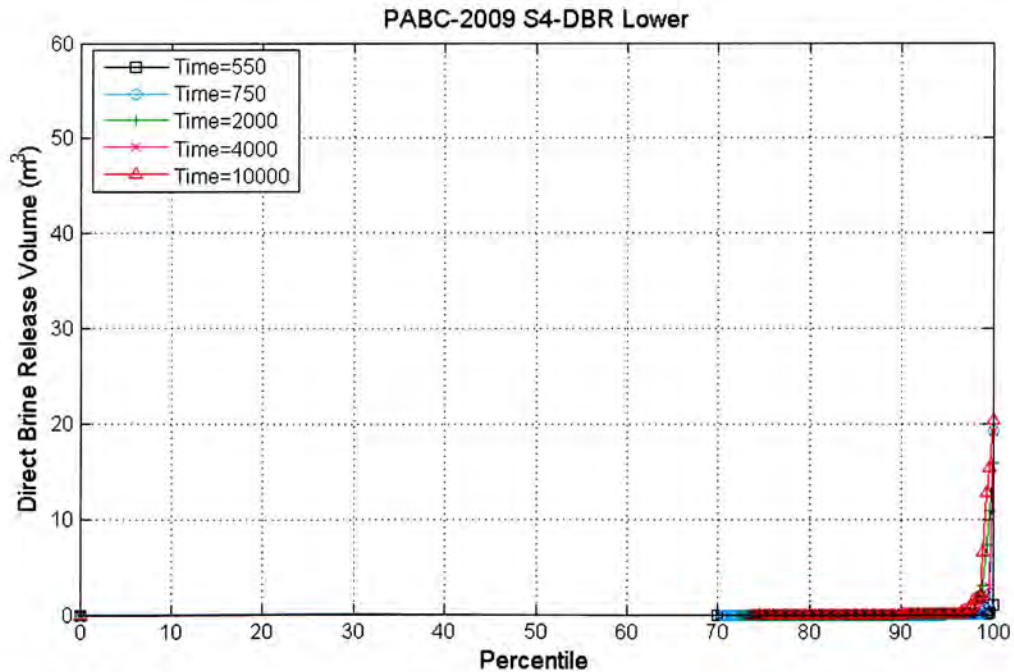


Figure 5-16: Plot of the percentile (x-axis) of DBR volumes that are less than the DBR volume on the y-axis for the PABC-2009 at the lower intrusion location for all replicates; scenario S4-DBR.

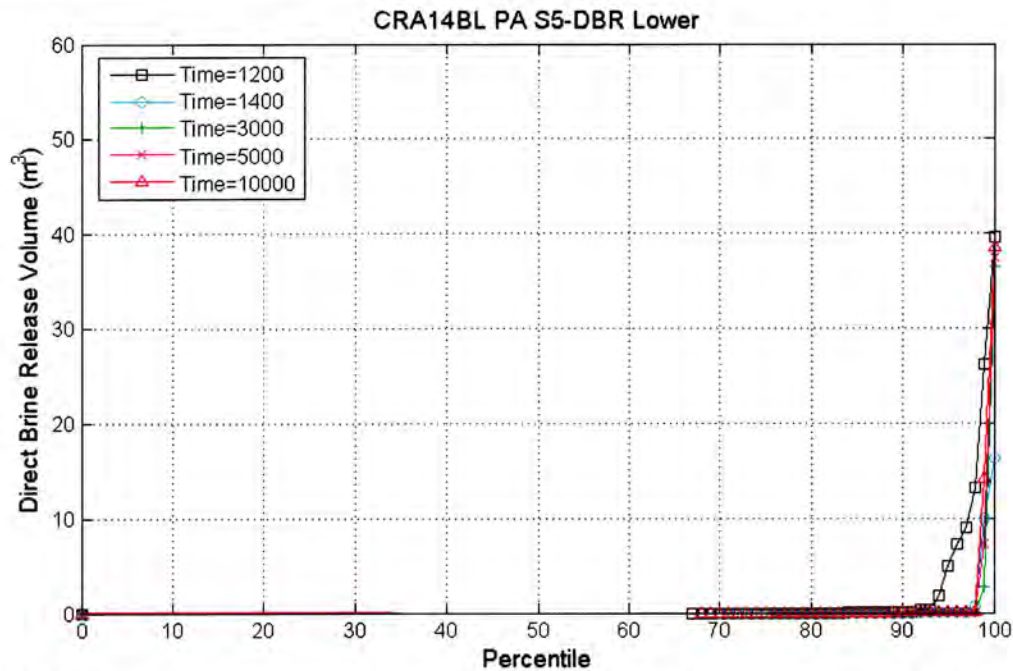


Figure 5-17: Plot of the percentile (x-axis) of DBR volumes that are less than the DBR volume on the y-axis for case CRA14-BL of the CRA-2014 PA at the lower intrusion location for replicate 1; scenario S5-DBR.

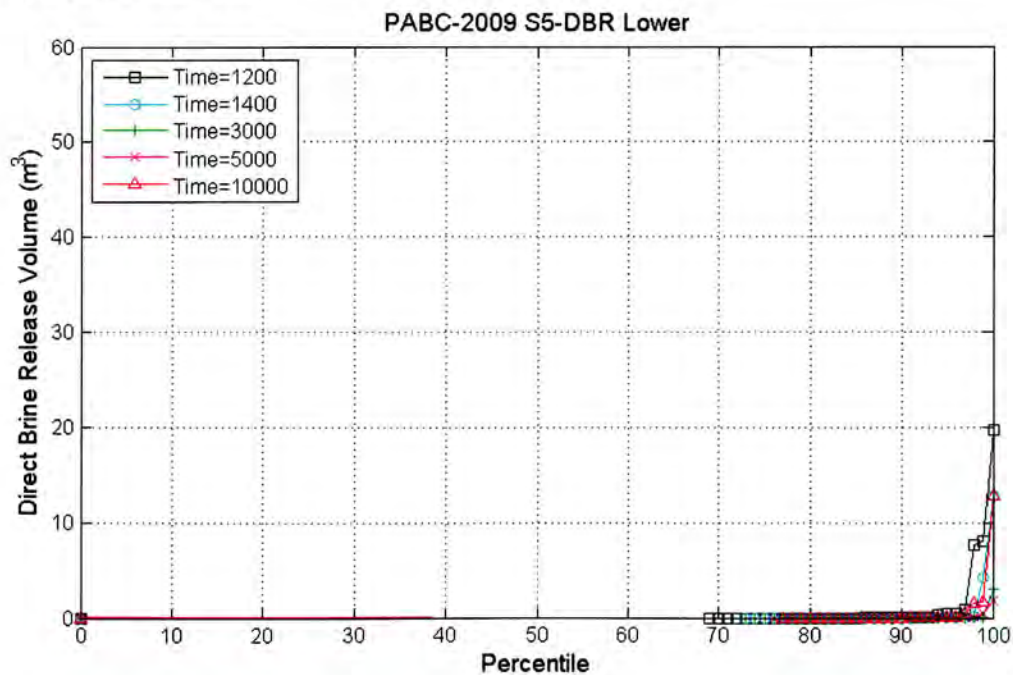


Figure 5-18: Plot of the percentile (x-axis) of DBR volumes that are less than the DBR volume on the y-axis for the PABC-2009 at the lower intrusion location for replicate 1; scenario S5-DBR.

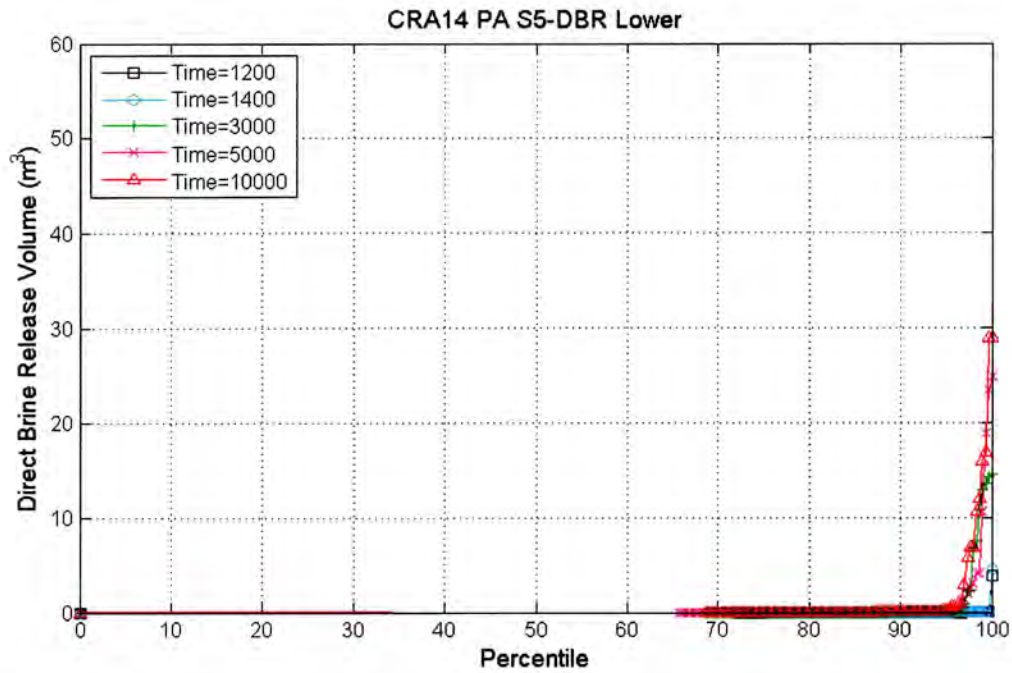


Figure 5-19: Plot of the percentile (x-axis) of DBR volumes that are less than the DBR volume on the y-axis for case CRA14-0 of the CRA-2014 PA at the lower intrusion location for all replicates; scenario S5-DBR.

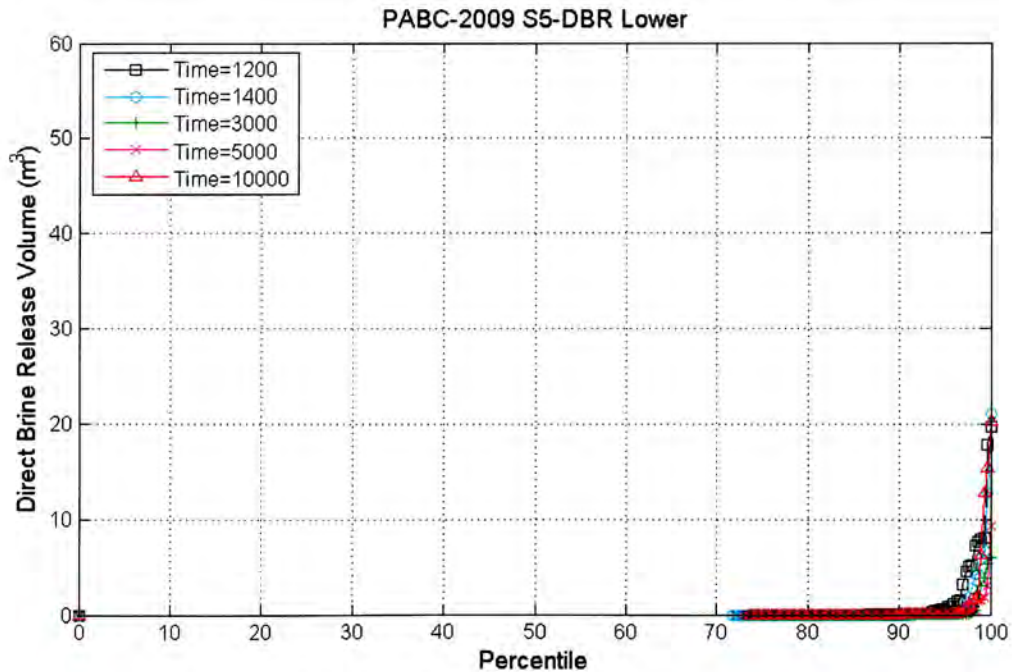


Figure 5-20: Plot of the percentile (x-axis) of DBR volumes that are less than the DBR volume on the y-axis for the PABC-2009 at the lower intrusion location for all replicates; scenario S5-DBR.

5.3 Sensitivity of Direct Brine Releases to Input Parameters

Volume averaged brine pressure and brine saturation in the intruded panel are the two most important variables that control DBR volumes (Clayton 2008). The sensitivity of the DBR volumes to these two variables is discussed qualitatively here. For the plots given below, the values of these parameters were extracted from the ALG2 files from the DBR calculations.

Scenarios S2-DBR and S3-DBR have significant DBR volumes because the presence of a previous borehole intrusion connecting the repository to the Castile brine reservoir has the general effect of simultaneously increasing the waste panel pressure and brine saturation. Hence, the sensitivity analysis presented here focuses on scenarios S2-DBR and S3-DBR because these scenarios have the greatest number of significant DBR volumes. As in previous DBR analyses performed hitherto, scenarios S1-DBR, S4-DBR, and S5-DBR have very few runs with non-zero DBR volumes and are thus excluded from the sensitivity analysis presented herein. Due to the close similarity between scenarios S2-DBR and S3-DBR, only scenario S2-DBR is discussed in the sensitivity analysis.

Volume averaged brine pressure in the intruded panel at the time of the intrusion is an important factor in determining occurrence of DBR. Figures 5-21 and 5-22 show scatter plots of DBR volume versus pressure in the intruded panel at different intrusion times for the case of a down-dip (lower) location of a drilling intrusion for cases CRA14-BL and CRA14-0, respectively, of the CRA-2014 PA. Figure 5-23 is a similar plot of the PABC-2009 results. As prescribed by the conceptual model, there are no DBRs until the brine pressure in the intruded panel exceeds the drilling fluid hydrostatic threshold of 8 MPa. This threshold is indicated in the figures by the solid vertical line. For the PABC-2009 and case CRA14-BL, above 8 MPa there is still a significant number of vectors having zero DBR volumes. Case CRA14-0 shows no vectors with zero brine volumes.

Some of the vectors plotted as having zero brine volumes in the PABC-2009 and case CRA14-BL have associated mobile brine saturations that are less than zero and thus no brine is available in a mobile form to be released (Clayton et al., 2010). Figures 5-24 through 5-26 show scatter plots of the same data as shown in Figures 5-21 and 5-23 but for different mobile brine saturation ranges. They show that DBR volumes tend to increase with increasing pressure and increasing mobile brine saturation, the variables to which DBR volumes are historically sensitive.

As the case was with the PABC-2009 results reported in Clayton et al. (2010) and reproduced here in Figures 5-23 and 5-26, case CRA14-0 results in Figures 5-22 and 5-25 show a clustering of the data about a linear trend (dashed line in the figures). The linear correlation is more pronounced, with less scatter about the average trend, in case CRA14-0 results than in the PABC-2009 and case CRA14-BL results, and has an appreciably different slope of about $6 \text{ m}^3/\text{MPa}$ compared to a slope of about $8 \text{ m}^3/\text{MPa}$ for the latter two cases. Comparing results in Figure 5-22 to those in Figure 5-25 indicates that linearity of the correlation between pressure and DBR volumes increases with increasing mobile brine saturation.

Figures 5-27 through 5-29 are plots of mobile brine saturation versus pressure for the S2-DBR scenario for all intrusion times with symbols indicating the range of DBR volumes, for cases

CRA14-BL, CRA14-0, and the PABC-2009, respectively. The results in these figures show the general increase in DBR volume with both brine saturation and pressure alluded to above, with only modest differences between case CRA14-BL and the PABC-2009 results. Case CRA14-0 results do not show any mobile brine saturation below the value of 0.2 indicated in Figure 5-28 by the dashed line.

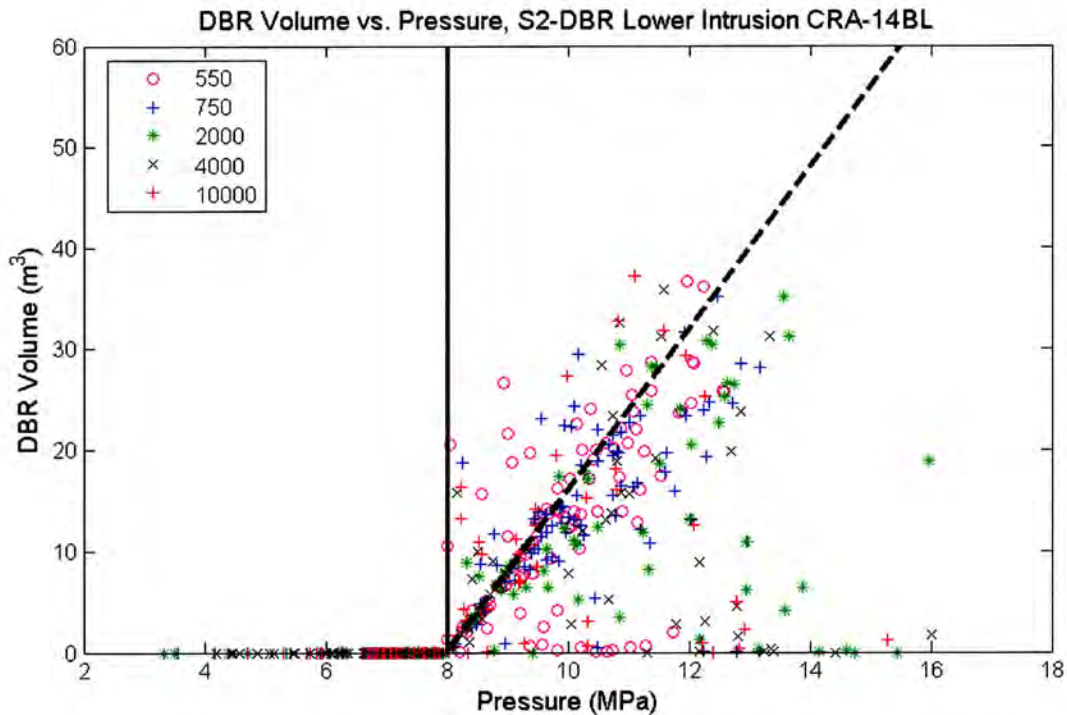


Figure 5-21: Scatter plot of DBR volume versus pressure in intruded panel for S2-DBR scenario, lower drilling intrusion, case CRA14-BL. Symbols indicate intrusion times in years.

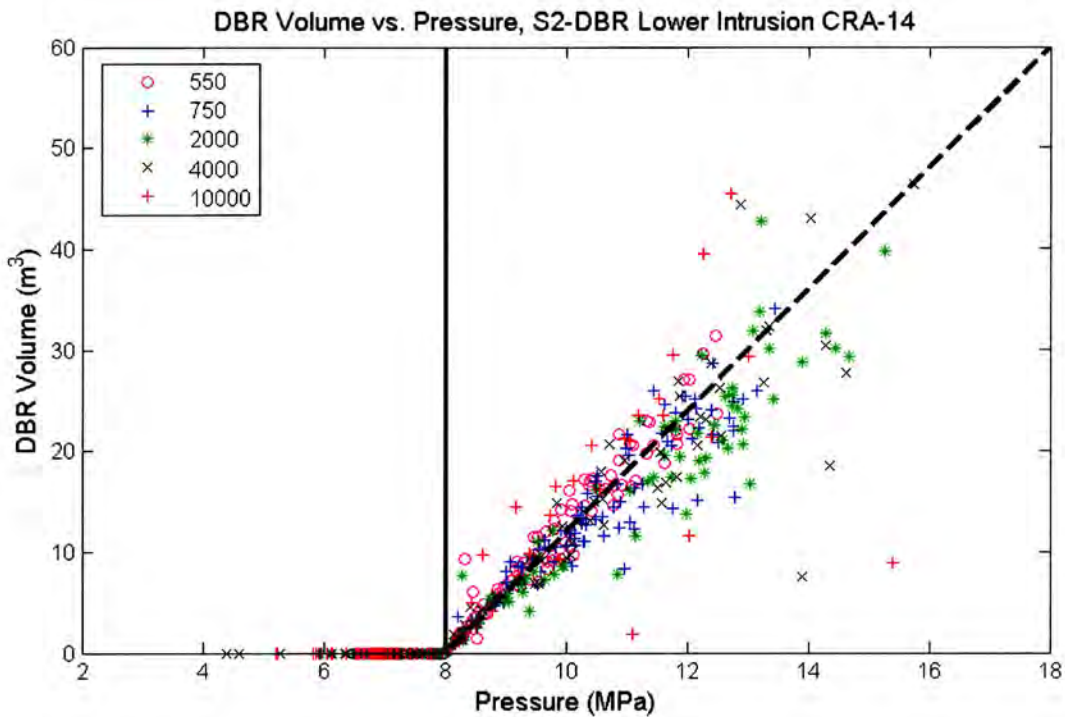


Figure 5-22: Scatter plot of DBR volume versus pressure in intruded panel for S2-DBR scenario, lower drilling intrusion, case CRA14-0. Symbols indicate intrusion times in years.

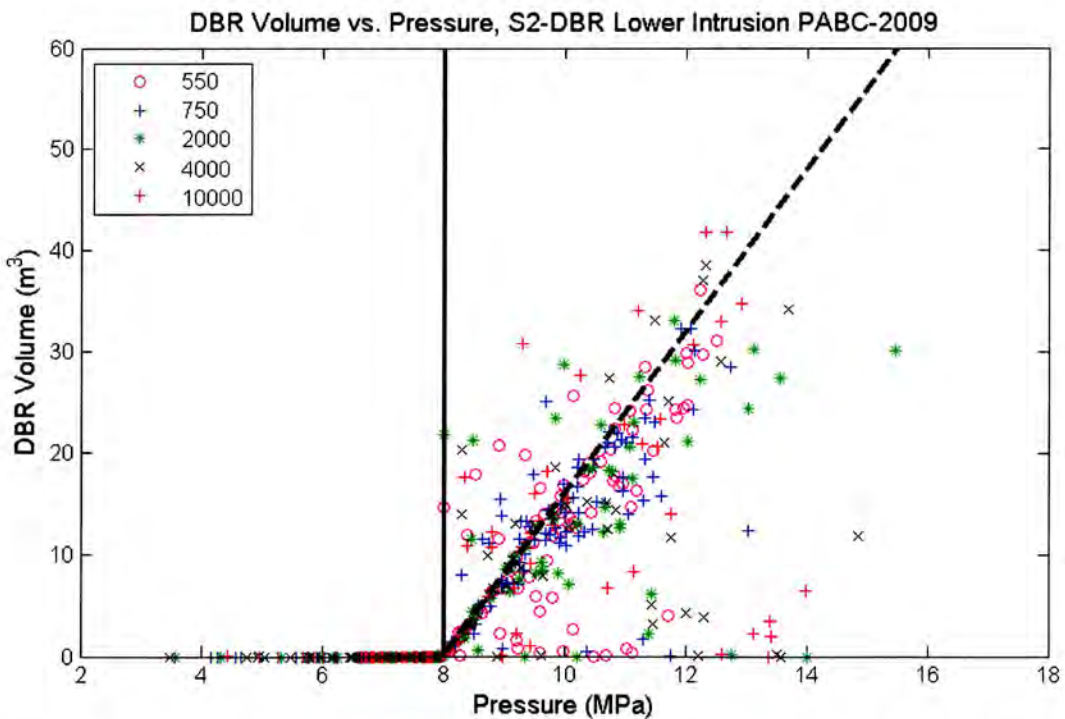


Figure 5-23: Scatter plot of DBR volume versus pressure in intruded panel for S2-DBR scenario, lower drilling intrusion, PABC-2009. Symbols indicate intrusion times in years.

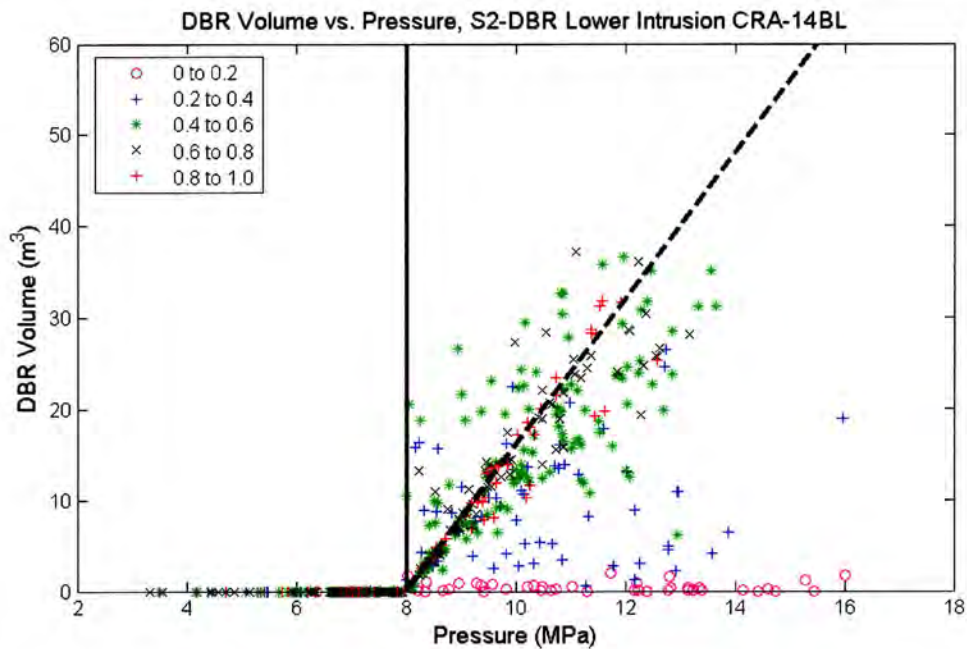


Figure 5-24: Scatter plot of DBR volume versus pressure in the intruded panel for replicate 1, S2-DBR scenario, lower drilling intrusion, CRA14-BL PA. Symbols indicate the range of mobile brine saturation (dimensionless).

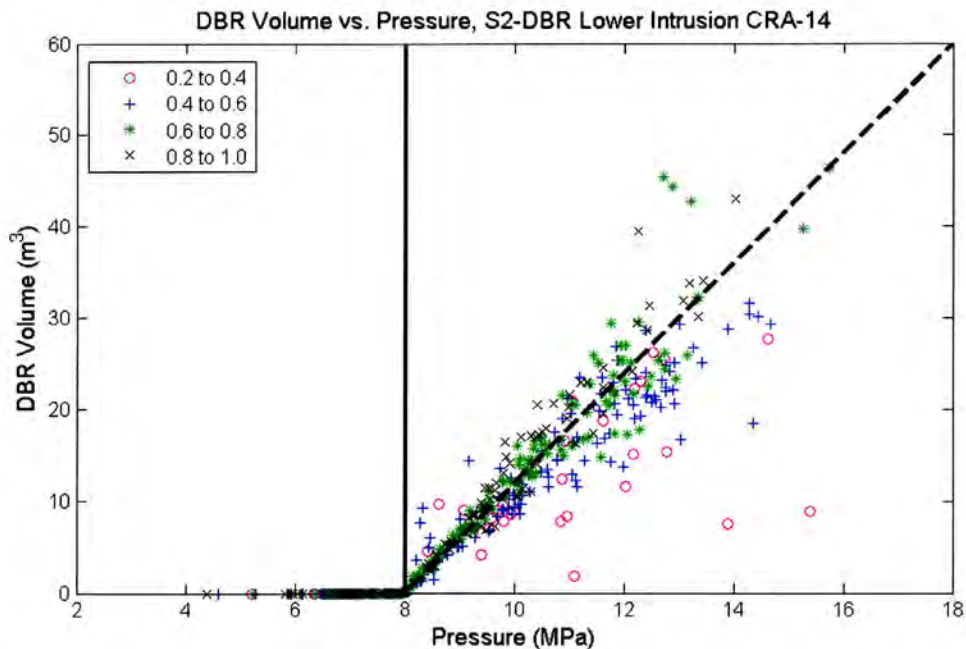


Figure 5-25: Scatter plot of DBR volume versus pressure in the intruded panel for replicate 1, S2-DBR scenario, lower drilling intrusion, CRA-2014 PA. Symbols indicate the range of mobile brine saturation (dimensionless).

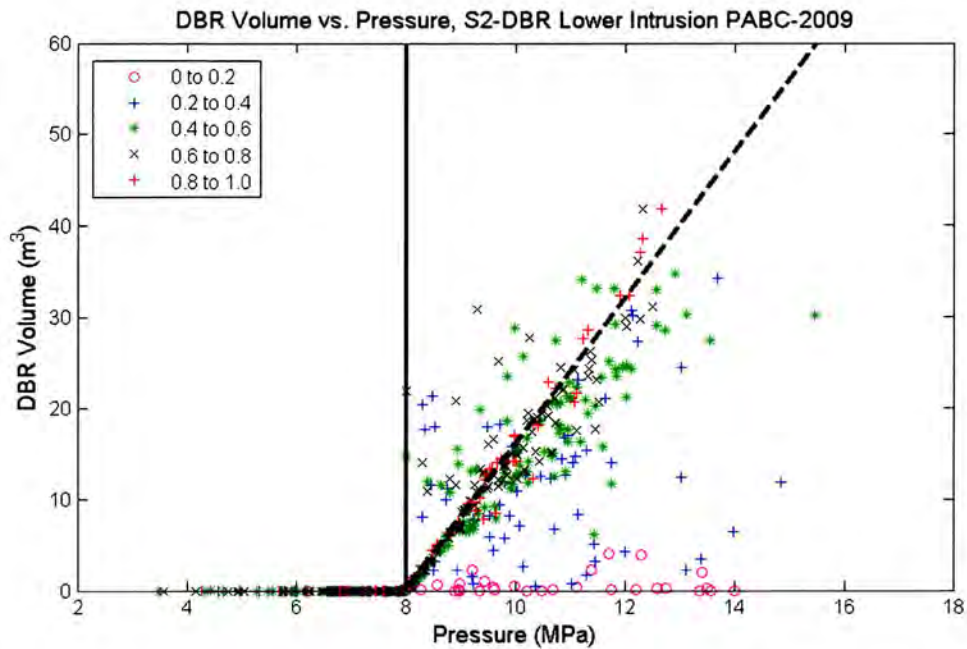


Figure 5-26: Scatter plot of DBR volume versus pressure in the intruded panel for replicate 1, S2-DBR scenario, lower drilling intrusion, PABC-2009. Symbols indicate the range of mobile brine saturation (dimensionless).

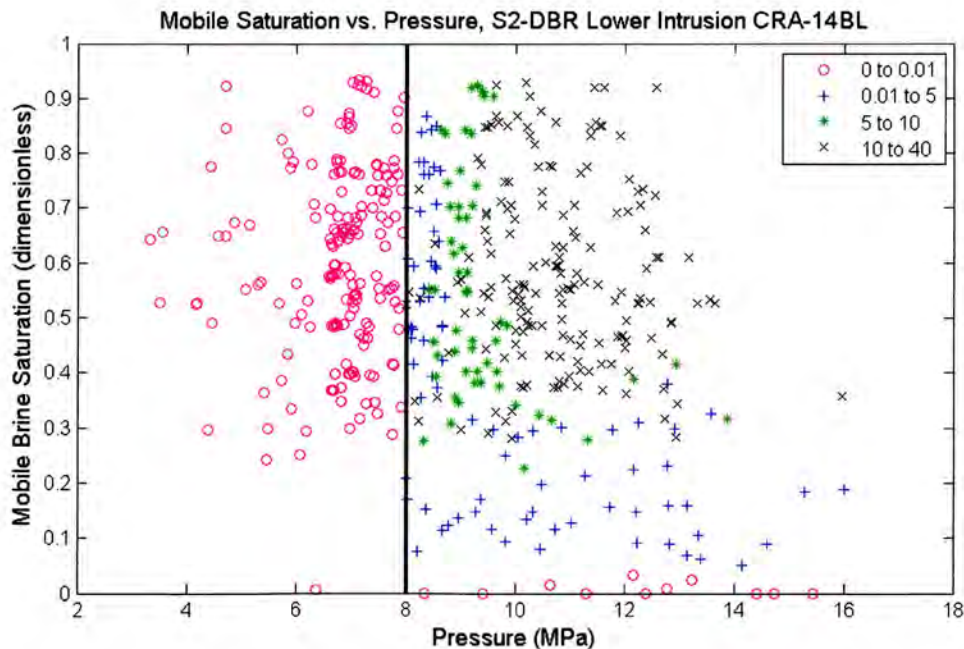


Figure 5-27: Scatter plot of mobile brine saturation versus pressure for replicate 1, S2-DBR scenario, lower drilling intrusion, all intrusion times, CRA14-BL PA. Symbols indicate the range of DBR volumes in m³.

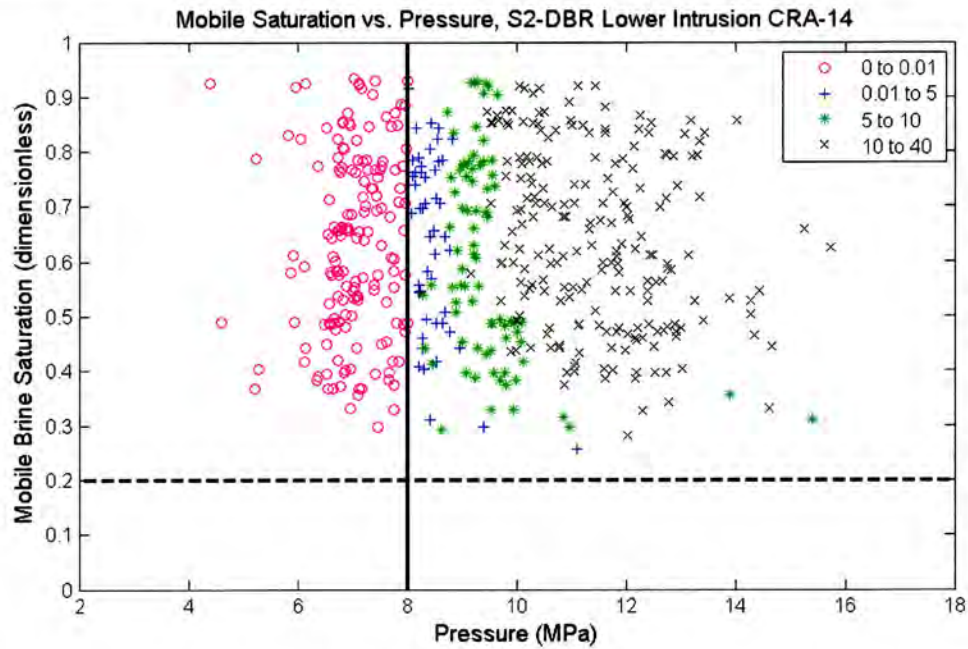


Figure 5-28: Scatter plot of mobile brine saturation versus pressure for replicate 1, S2-DBR scenario, lower drilling intrusion, all intrusion times, CRA-2014 PA. Symbols indicate the range of DBR volumes in m^3 .

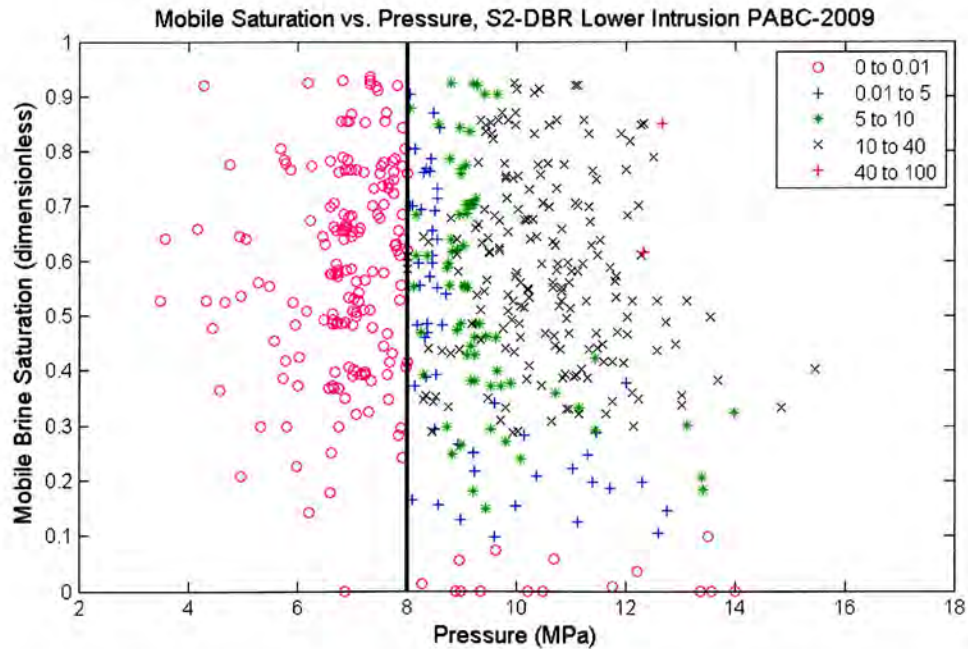


Figure 5-29: Scatter plot of mobile brine saturation versus pressure for replicate 1, S2-DBR scenario, lower drilling intrusion, all intrusion times, PABC-2009. Symbols indicate the range of DBR volumes in m^3 .

6 CONCLUSIONS

The DBR results from the overall CRA-2014 PA (case CRA14-0) show appreciable changes from those of the PABC-2009. They still indicate that direct brine releases to the surface are very unlikely for most intrusions into the repository and that, in most cases, such intrusions result in non-zero but inconsequential DBR volumes. The exception to this statement is for intrusions into a panel that had previously been intruded by a borehole that had also intersected an underlying pressurized Castile brine reservoir. Such intrusions are represented in PA by the lower drilling intrusions in the scenarios S2-DBR and S3-DBR. Based on a comparison of the results from the CRA-2014 PA to those from the PABC-2009, it is concluded that the CRA-2014 PA although the maximum DBR volumes are higher for each scenario, the frequency of DBR releases and the variability in DBR volumes are appreciably lower. As in previous analyses, these results have been explained in terms of the parameters that affect DBR volumes, as well as by the changes in parameter values (including the iron corrosion rate), the panel closure system, the mined-out volume, and the refined water budget implementation.

7 REFERENCES

Brooks, R.H. and A.T. Corey. 1964. Hydraulic properties of porous media, Hydrology Paper no. 3, Civil Engineering Department, Colorado State University, Fort Collins, CO.

Camphouse, R.C. 2013a. Analysis Plan for the 2014 WIPP Compliance Recertification Application Performance Assessment. Sandia National Laboratories, Carlsbad, NM. ERMS 559198.

Camphouse, R.C. 2013b. Analysis Package for Salado Flow Modeling done in the 2014 Compliance Recertification Application Performance Assessment (CRA-2014 PA). Sandia National Laboratories, Carlsbad, NM. ERMS 559980.

Camphouse, R.C. 2012a. Analysis Plan for the 2012 WIPP Panel Closure System Performance Assessment. AP-161, Revision 0. Sandia National Laboratories, Carlsbad, NM. ERMS 557726.

Camphouse, R.C. 2012b. Analysis Package for Salado Flow Modeling Done in the AP-161 (PCS-2012) Performance Assessment. Sandia National Laboratories, Carlsbad, NM. ERMS 558204.

Camphouse, R.C., D.C. Kicker, T.B. Kirchner, J.J. Long, B. Malama, T.R. Zeitler. 2012. Summary Report and Run Control for the 2012 WIPP Panel Closure System Performance Assessment. Sandia National Laboratories, Carlsbad, NM. ERMS 558365.

Chappelear, J.E. and A.S. Williamson. 1981. Representing Wells in Numerical Reservoir Simulation. ERMS 249488.

Clayton, D.J. 2008. Analysis Package for Direct Brine Releases: Compliance Recertification Application – 2009. Sandia National Laboratories, Carlsbad, NM. ERMS 548571.

Clayton, D.J., S. Dunagan, J.W. Garner, A.E. Ismail, T.B. Kirchner, G.R. Kirkes, M.B. Nemer. 2008. Summary Report of the 2009 Compliance Recertification Application Performance Assessment. Sandia National Laboratories, Carlsbad, NM. ERMS 548862.

Clayton, D.J. 2010. Analysis Package for Direct Brine Releases: CRA-2009 Performance Assessment Baseline Calculation, Revision 0. Sandia National Laboratories. Carlsbad, NM. ERMS 552829.

Clayton, D.J., R.C. Camphouse, J.W. Garner, A.E. Ismail, T.B. Kirchner, K.L. Kuhlman, and M.B. Nemer. 2010. Summary Report of the CRA-2009 Performance Assessment Baseline Calculation. Sandia National Laboratories, Carlsbad, NM. ERMS 553039.

Cotsworth, E. 2005. EPA Letter on Conducting the Performance Assessment Baseline Change (PABC) Verification Test. U.S. EPA, Office of Radiation and Indoor Air, Washington, D.C. ERMS 538858.

Cotsworth, E. 2009. EPA Letter on CRA-2009 First Set of Completeness Comments. U.S. EPA, Office of Radiation and Indoor Air, Washington, D.C. ERMS 551444.

Garner, J.W. 2010. Analysis Package for PANEL: CRA-2009 Performance Assessment Baseline Calculation. Sandia National Laboratories, Carlsbad, NM. ERMS 553032.

Helton, J.C, J.E. Bean, F.W. Berglund, F.J. Davis, K. Economy, J.W. Garner, J.D. Johnson, R.J. MacKinnon, J. Miller, D.G. O'Brien, J.L. Ramsey, J.D. Schreiber, A. Shinta, L.N. Smith, D.M. Stoelzel, C. Stockman and P. Vaughn. 1998. Uncertainty and Sensitivity Analysis Results Obtained in the 1996 Performance Assessment for the Waste Isolation Pilot Plant. Sandia National Laboratories, Albuquerque, NM. SAND98-0365, ERMS 252619.

Lee, J. 1982. Well Testing. SPE Textbook Series Vol. 1. New York, NY: Society of Petroleum Engineers of AIME.

Leigh, C.D., J.F. Kanney, L.H. Brush, J.W. Garner, G.R. Kirkes, T. Lowry, M.B. Nemer, J.S. Stein, E.D. Vugrin, S. Wagner, and T.B. Kirchner. 2005. 2004 Compliance Recertification Application Performance Assessment Baseline Calculation, Revision 0. Sandia National Laboratories, Carlsbad, NM. ERMS 541521.

Long, J.J. 2013. Execution of Performance Assessment Codes for the CRA-2014 Performance Assessment. Sandia National Laboratories, Carlsbad, NM. ERMS 560016.

Malama, B. 2012. Analysis Package for Direct Brine Releases: 2012 Panel Closure System Performance Assessment (PCS-2012 PA). Sandia National Laboratories, Carlsbad, NM. ERMS 558226.

Mattax, C.C. and R.L. Dalton. 1990. Reservoir Simulation. Henry L. Doherty Memorial Fund Society of Petroleum Engineers Inc., Richardson, TX.

MacKinnon, R.J., and G. Freeze. 1997a. Summary of EPA-Mandated Performance Assessment Verification Test (Replicate 1) and Comparison With the Compliance Certification Application Calculations, Revision 1. Sandia National Laboratories, Carlsbad, NM. ERMS 422595.

MacKinnon, R.J., and G. Freeze. 1997b. Summary of Uncertainty and Sensitivity Analysis Results for the EPA-Mandated Performance Assessment Verification Test, Rev. 1. Sandia National Laboratories, Carlsbad, NM. ERMS 420669.

MacKinnon, R.J., and G. Freeze. 1997c. Supplemental Summary of EPA-Mandated Performance Assessment Verification Test (All Replicates) and Comparison With the Compliance Certification Application Calculations, Revision 1. Sandia National Laboratories, Carlsbad, NM. ERMS 414880.

Pasch, J. and C. Camphouse, 2011. Analysis Package for Direct Brine Releases: Panel Closure Redesign and Repository Reconfiguration Performance Assessment (PC3R PA), Revision 0. Sandia National Laboratories. Carlsbad, NM. ERMS 555249.

Information Only

Stoelzel, D.M. and D.G. O'Brien. 1996. Conceptual Model Description of BRAGFLO Direct Brine Release Calculations to Support the Compliance Certification Application (CCA MASS Attachment 16-2). U.S. Department of Energy, Carlsbad, NM. ERMS 239090.

U.S. Congress. 1992. WIPP Land Withdrawal Act, Public Law 102-579, 106 Stat. 4777, 1992; as amended by Public Law 104-201, 110 Stat. 2422, 1996.

U.S. Department of Energy (DOE) 2004. Title 40 CFR Part 191 Compliance Recertification Application for the Waste Isolation Pilot Plant, 10 vols., U.S. Department of Energy Waste Isolation Pilot Plant, Carlsbad Area Office, Carlsbad, NM. DOE/WIPP 2004-3231.

U.S. Environmental Protection Agency (EPA). 1998. 40 CFR 194, Criteria for the Certification and Recertification of the Waste Isolation Pilot Plant's Compliance with the Disposal Regulations: Certification Decision: Final Rule. Federal Register, Vol. 63, 27354-27406. ERMS 251924.

U.S. Environmental Protection Agency (EPA). 2006. 40 CFR 194, Criteria for the Certification and Recertification of the Waste Isolation Pilot Plant's Compliance with the Disposal Regulations: Certification Decision: Final Rule, Federal Register. Vol. 71, 18010-18021.

U.S. Environmental Protection Agency (EPA). 2010. 40 CFR Part 194 Criteria for the Certification and Recertification of the Waste Isolation Pilot Plant's Compliance With the Disposal Regulations: Recertification Decision, Federal Register No. 222, Vol. 75, pp. 70584-70595, November 18, 2010.

Information Only